FIRST AND SECOND LAW ANALYSES OF A LARGE BORE TWO STROKE SPARK IGNITION ENGINE FUELED WITH NATURAL GAS

A Thesis

by

ABDULLAH UMAIR BAJWA

Submitted to the Office of Graduate and Professional Studies of
Texas A&M University
in partial fulfillment of the requirements for the degree of

MASTER OF SCIENCE

Chair of Committee,	Tim Jacobs
Committee Members,	Jerald Caton
	Adonios N. Karpetis
Head of Department,	Andreas A. Polycarpou

December 2016

Major Subject: Mechanical Engineering

ABSTRACT

A zero dimensional thermodynamic model with no spatial resolution has been developed to analyze the effectiveness of energy and exergy utilization in a large bore, single cylinder, two-stroke engine. Exergy analysis was performed to supplement energy analysis to gain deeper insights into the exploitation of the essence of energy during engine operation. The closed and the open portions of the cycle were modeled in this study using theory of gas dynamics and thermodynamics. Suitable forms of the first and second laws of thermodynamics were applied to a two zone (burned and unburned) control mass during the closed portion of the cycle and control volume during the open portion of the cycle, respectively. A Wiebe function describes the fuel burning rate and was used to simulate combustion. All simulated results were validated using experimental data. Exergy transfers in and out of the system accompanying chemical reactions, work, heat transfer and flows were traced and the major sources of exergy destruction (irreversibilities) identified. Major findings from the analysis were that 14% of the fuel's exergy was destroyed because of combustion and almost half (46%) of the initial exergy is lost with exhaust gases. Compared to four stroke engines the percentage exergy destruction is relatively less because of lower cylinder temperatures. These findings highlight shortcomings in the thermodynamic design of the engine and help direct future research efforts.

ACKNOWLEDGEMENTS

I would like to thank my committee chair and my academic adviser, Dr. Tim Jacobs for being a mentor to me throughout my stay at Texas A&M and for guiding and supporting me throughout the course of this research. I would also like to thank Dr Jerald Caton and Dr Eric Petersen for their support in troubleshooting bugs in the thermodynamics and gas dynamics models, respectively.

Thanks also go to my colleagues at AERL for their continued support throughout my research. Especially, Alireza Mashayekh, Jeff Brown and Aaron Griffin for helping me collect experimental data which was needed for validation of my simulation models.

I would like to acknowledge the Fulbright Scholars Program for providing financial support for my graduate studies and GE Oil and Gas for their technical and financial support.

Finally, thanks to my friends and family for their encouragement throughout my educational career.

NOMENCLATURE

A	Exergy
a	Specific Exergy
A_{ch}	Chemical Exegy
aTDC	After Top Dead Center
BDC	Bottom Dead Center
CAD	Crank Angle Degrees
C_D	Coefficient of Discharge
EPC	Exhaust Port Closing
EPO	Exhaust Port Opening
g	Gibbs Function
h	Specific Enthalpy
h_c	Heat Transfer Coefficient
I	Irreversibility
IPC	Intake Port Closing
IPO	Intake Port Opening
k	Specific Heat Ratio
m	Mass
mfb	Mass Fraction Burned
n	Wiebe Parameter
P	Pressure

Q	Heat Transfer
r	Residual Fraction
ROHR	Rate of Heat Release
S	Entropy
SOC	Start of Combustion
T	Temperature
TDC	Top Dead Center
u	Specific Internal Energy
u_p	Mean Piston Speed
V	Volume
W	Work
x	Mass Fraction Burned

Greek and Other Symbols:

θ	Crank angle
θ_s	Start of Combustion Angle
θ_b	Burn Duration Angle
μ	Chemical Potential

Superscripts:

o	True dead state

Subscripts:

b	Burned
f	Fuel
LHV	Lower Heating Value
o	Restricted Dead State
u	Unburned

TABLE OF CONTENTS

LIST OF FIGURES

LIST OF TABLES

1. INTRODUCTION

1.1. Motivation

Two-stroke engines have been around for over a century now. Sir Duglad Clerk is credited with inventing the first two-stroke engine [1]. Reliability in operation resulting from simple mechanical design is the main reason why the two-stroke engine has survived to this day, despite having poor gas exchange performance compared to its four-stroke counterparts. Approximately 15% to 40% of the fuel-air mixture is exhausted out of two-stroke engines without taking part in combustion [2]. Back in the day when these engines, including the 'legacy engine' being investigated in this study, were designed, engine reliability and performance were the main design criteria. Fuel conversion efficiency and emissions performance weren't a big concern. In the post-emissions regulated world of today for some applications the fuel conversion efficiency might still not be a concern but the emissions performance of the engine can no longer be ignored.

Developing engineering tools to investigate emissions, operating and efficiency performance of the engine was the main motivation behind starting this study. The emissions performance of the engine is strongly linked to the thermodynamic behavior of the cylinder gases. Thermodynamic models based on the first and second laws developed in this project give us a glimpse of the thermodynamic behavior of cylinder gases. These findings can help the engine designer of today to incorporate improvements

in engine design and/or operating regime to improve engine emissions while maintaining acceptable levels of engine reliability and efficiency.

1.2. Background

1.2.1. History and Applications of Two Stroke Engines

Two-stroke engines are used in a wide array of applications. In the early days most of its applications were limited to the automotive sector where they were the engine of choice to power motorcycles. Their demand peaked in the later half of the twentieth century but afterwards it took a hit because of legislative pressure on manufacturers to control exhaust emissions, which compelled them to look towards four-stroke engines. Two stroke engines have also been used to drive cars, trucks, locomotives, ships, tanks and even aircrafts e.g. the Napier Nomad [1]. Major applications where two stroke engines are employed today include: handheld power tools e.g. chainsaws, lawn mowers, remote controlled aircrafts; water sports vehicles e.g. jet skis and as prime-movers for natural gas compressors at compressor stations which maintain pressure in the gas supply pipelines.

1.2.2. The Two Stroke Cycle

A cross sectional view of the two-stroke engine used in this study is shown in Figure 1. The simplistic geometry of the engine is representative of a typical naturally aspirated, ported, cross-scavenged two-stroke engine. Thus, it has been chosen to explain

two-stroke engine operation. All gas exchange processes are controlled by the edges of the piston based upon whether they are covering the gas exchange ports or not.

Air and fuel enter the stuffing box (scavenging chamber) through an air inlet port and a reed valve, respectively (Figure 1). Strips in the reed valve act as check valves and ensure the unidirectional flow of natural gas into the engine. Their opening and closing is controlled by the pressure difference between the cylinder and the fuel line pressure. When the piston is close to the TDC, vacuum created in the stuffing box (Figure 1) is strong enough to cause the reed valve to open. This causes fresh fuel to be inducted and mix with incoming air.

As the piston moves towards the BDC, scavenging ports (six for the current engine) are uncovered and the air fuel mixture is pushed into the main cylinder. Here it undergoes combustion and is expelled through four exhaust ports located across the cylinder from the scavenging ports. The rush of incoming fresh air fuel mixture from the stuffing box aids in the expulsion of the burnt mixture. During this process, some of the fresh mixture because of its momentum escapes directly through the exhaust ports and a portion of the potentially useful combustible gas mixture is lost. This inefficient gas exchange process is known as scavenging and has been shown in Figure 2. This inefficiency in the gas exchange is quantified by the trapping efficiency of the engine, which is a ratio of the mass of the gas mixture that was retained in the cylinder at the end of the gas exchange process to the mass of the gas mixture that was supplied.

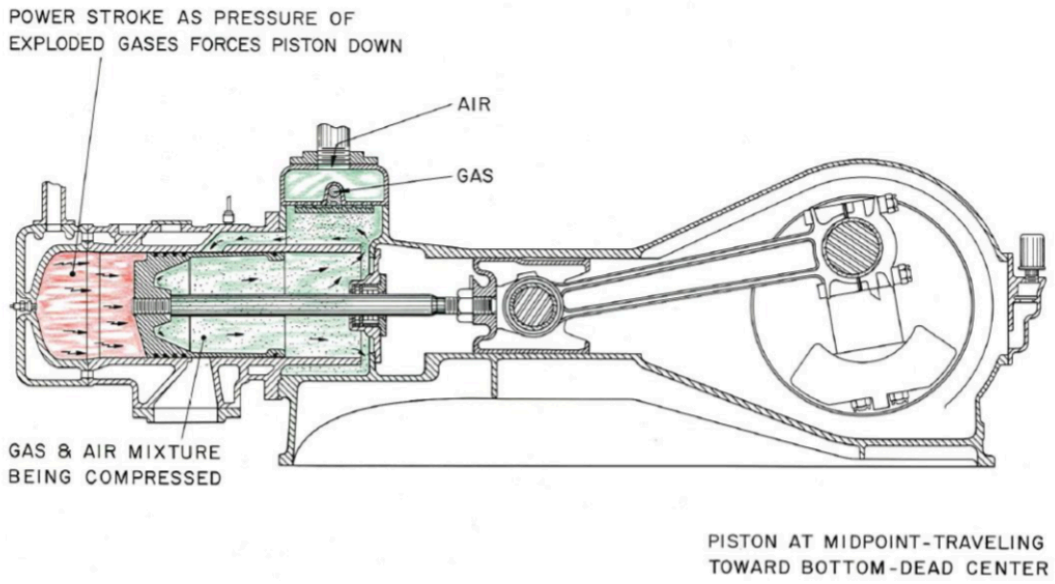

Figure 1: Cross sectional view of a cross-scavenged two-stroke engine. Red denotes combustion mixture and green denotes fresh charge [3].

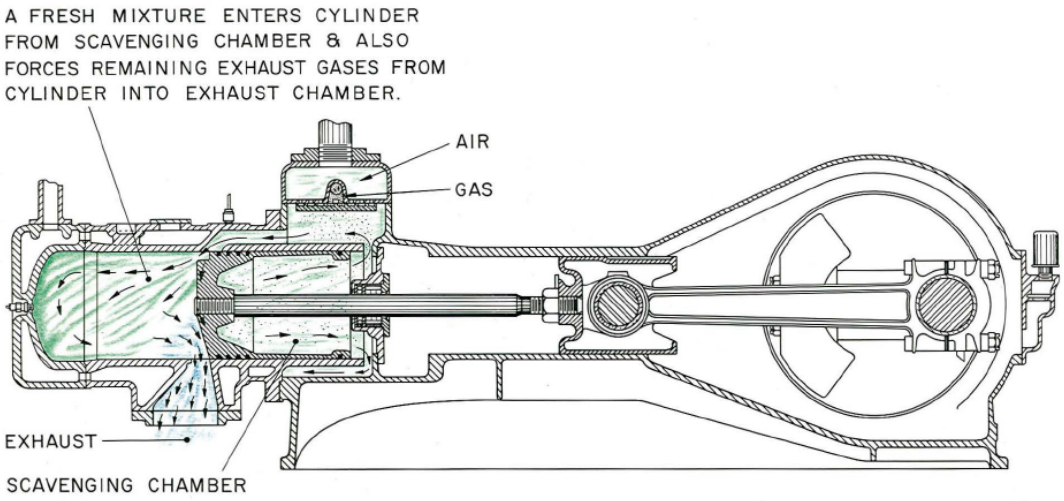

Figure 2: Cross sectional view of a cross-scavenged two-stroke engine illustrating the scavenging process. Blue signifies exhaust gases. Piston is at BDC [3].

The current engine is a crank case compression engine with a cross cylinder scavenging regime (Figure 3). Other popular scavenging regimes include the loop and modified loop (Schnurie) regimes.

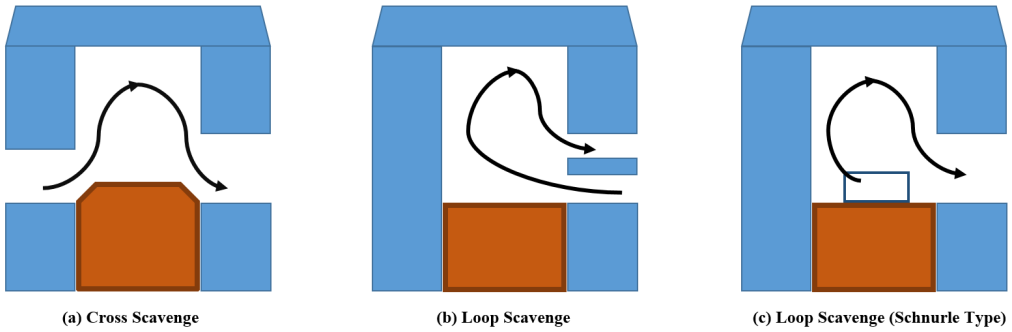

Figure 3: Various two-stroke engine scavenging regimes [4]

1.2.3. Advantages of Two-Stroke Engines

Two stroke engines have the potential for higher power densities compared to their four stroke counterparts with a power stroke at each revolution of the crankshaft as opposed to one per every two revolutions. Moreover, the relatively simple and robust design capable of operating reliably in harsh conditions makes the two-stroke engine an attractive option for several applications. One such application is driving reciprocating compressors to pump natural gas through pipelines. Here, the shortcomings of the two-stroke design in regards to poor volumetric efficiencies and high emission are outweighed by the aforementioned advantages. Because of these reasons for more than half a century large bore two-stroke engines have been and continue to be the prime mover of choice in the oil field services industry.

Because of their extraordinarily dependable operation under unpredictable and rough operating conditions experienced in natural gas fields, the engine designs developed in the first half of the twentieth century continue to operate with no major design changes. One such design is the single-cylinder large bore spark ignited cross-scavenged engine, which was designed in the 1960s. With modern-day advanced experimental and computational tools, a series of investigations has been initiated to develop a better understanding of the various thermos-fluid phenomenon taking place within the engine and study their influence on the engine's emissions and operating performance.

1.3. Objective

The objective of this study is to develop a computationally inexpensive simulation platform, which provides the two-stroke engine researcher with necessary tools to be able to gain an insight into the thermodynamics of the engine. This model would serve as the first step in the design improvement process to bring these 'legacy' engines compliant with the regulatory requirements of today. The next steps would include detailed CFD modeling and experimental investigations. The current model will be structured in such a way that new sub-functions serving various requirements can be easily added to the basic foundational code. Thus, making the code a versatile tool capable of being used in multiple investigations on the engine.

For the current project this modeling framework will be used to carry out a second law analysis on the engine in order to get a deeper understanding of the exergy

transfers within the engine. Exergy transfer contributions from various thermal energy flows (heat transfer, mass flows, work, irreversibilities) will be listed individually and their impact on the overall exergy utilization discussed.

2. LITERATURE REVIEW

2.1. Engine Modeling

Engine modeling using the theories of thermodynamics, gas dynamics, fluid mechanics and heat transfer is a well-established field and has been around for over 50 years [5]. Both spark ignition engines [6] [7] [8] [9] and compression ignition engines [10][11] [12] have been modeled using various modeling approaches. Engine operation using different fuels has also been simulated [13][14]. Engine models can be characterized based on numerous criteria. A few of these have been discussed below.

2.1.1. Number of Zones

The first criteria to characterize engine models is the number of zones in the cylinder gases being modeled. A zone represents a volume of gas within the cylinder that has uniform thermodynamic properties (temperature, pressure, internal energy and enthalpy etc.). These properties can, however, vary across zones. For the sake of computational ease, simplifying assumptions like uniform pressure across all zones are normally incorporated in the analysis. Depending on the desired accuracy, cylinder gases can be divided into multiple zones and the laws of thermodynamics are applied separately to each zone. If it is reasonable to assume that the whole gas mixture is homogenous in terms of composition and thermodynamic properties, a single zone model would suffice [10] [12] [13]. Two zone models are used to split the gas volume into a burned and an unburned zone. Numerous such models have been developed for four stroke engines [15] [12]. They can be modified to work with two-stroke engines

too. Three zone models comprising of a burned zone boundary layer, a burned zone adiabatic core and an unburned zone have also been developed [16] [6] [7]. They offer improved accuracy for NOx predictions from homogenous charge engines. This modification serves as future work. Caton [17] has discussed the implications of using multi-zone models on emissions (NOx) generation and exergy transfers/ production compared to single-zone models. Ramos [18] has also carried out a similar comparative study using a one-dimensional model.

2.1.2. Spatial Resolution

Another basis for characterization of thermodynamic models is the degree of spatial resolution it provides. Models range for zero-dimensional models [3] [19] [18] with no spatial resolution to detailed three-dimensional models [20] [21] with complete spatial resolution. This additional resolution comes at added computational cost. Detailed 3D modeling normally falls in the computational fluid dynamics domain and detailed sub models which capture cylinder fluid dynamics (swirl, squish, tumble and turbulence) as well as chemistry of the gas mixture have to be incorporated. The current model like many other thermodynamic models is a 0-D model where it is assumed that spatially there are no thermodynamic gradients within each zone. For studies, such as the one presented here, it is reasonable to opt for the 0-D approach because in the context of thermodynamic calculations spatial gradients aren't significant enough to influence the final results substantially. This is why sometimes 0-D models are simply referred to as thermodynamic models and higher dimensional models are referred to by their

dimensionality [18]. Zero or quasi-dimensional models [22] [9] can provide a reasonably accurate big picture view of the thermodynamic behavior of bulk cylinder gases at different crank angle degrees. This is possible because the various sub-models working in the background, like rate of combustion calculator, are not phenomenological in nature but, are rather empirical models developed by engine experimentalists. The empirical correlations are tuned to fit the behavior of the engine being modeled. Quasi-dimensional models are a notch more sophisticated than 0-D models because they have some sense of the location of flame front initiation and propagation path [23].

2.1.3. Combustion Model

Once a combustible fuel air mixture is present in the cylinder and conditions are suitable for ignition, combustion ensues and unburned fuel reacts with air to form combustion products. Irrespective of the number of zones in the model and the dimensionality of the model a function that prescribes the rate at which unburned fuel is being converted into combustion products is required. This function outputs *mass fraction burned (x)* at different crank angle degrees. As the name suggests, 'x' is the ratio of mass of fuel that has been burned to the total mass of the fuel available before combustion.

$$x = \frac{(m_f)_{burned}}{(m_f)_{total}} \qquad (1)$$

Combustion depends on multiple factors. Some of them include: engine geometry, fuel's chemical properties, fuel-air equivalence ratio, start of ignition, combustion chamber geometry, flame propagation characteristics (laminar flame speed, turbulence intensity, transfer properties) and engine's operating conditions. A good combustion model is supposed to capture the effects of all of these parameters, but because of the complex nature of combustion phenomenon empirical correlations are sometimes used to mathematically model combustion. All the aforementioned factors that influence combustion are captured by tuning parameters present in these correlations. The most popular of these functions is the Wiebe function [24]. The mathematical form of the function is given by equation 2.

$$x(\theta) = 1 - \exp\left\{-a\left(\frac{(\theta-\theta_s)^n}{\theta_b}\right)\right\} \qquad (2)$$

'a' and 'n' are the tunable parameters which are used to match calculated mass fraction to experimentally obtained fraction. 'Θ' is the instantaneous crank angle degree, 'Θ_s' is the crank angle at which combustion starts and 'Θ_b' is the burn duration in crank angle degrees. Start and end of combustion are estimated from experimental mass fraction burned profiles at the 1% and 99% mass burnt points, because the combustion duration obtained using 10% and 90% points is significantly smaller than the former.

Another mass fraction burned function sometimes used is the sinusoidal function. It is expressed by equation (3) [15]:

$$x(\theta) = \frac{1}{2}\{1 - \cos\left(\frac{\theta - \theta_s}{\theta_b}\right)\} \quad (3)$$

The term "experimentally obtained mass fraction burned" should be used cautiously, because it is not a directly measured quantity. In fact, experimental 'x' is calculated from rate of heat release profiles, which in turn are calculated by applying the first law of thermodynamics to experimental pressure curves. Heywood [25] has described a way to calculate experimental mass fraction burned.

Irrespective of how the mass fraction burned profile is obtained the burning behavior of fuel should be qualitatively similar. They form an 's' shaped curve ranging between 0 and 1. 0 mass fraction burned means that combustion hasn't started and all of the fuel is unburned. A value of 1 for 'x' means that all of the fuel exists as burned combustion products. In the beginning i.e. right after 'θ_s', the combustion proceeds slowly because of relatively low mixture temperatures and turbulence. This phase is referred to as the flame development phase. This is followed by a rapid burn phase during which bulk of the fuel is burned. In the latter portion the fuel burning rate slows down again because the reactants are no longer readily available and cooling caused by expansion. Figure 4 illustrates this combustion behavior.

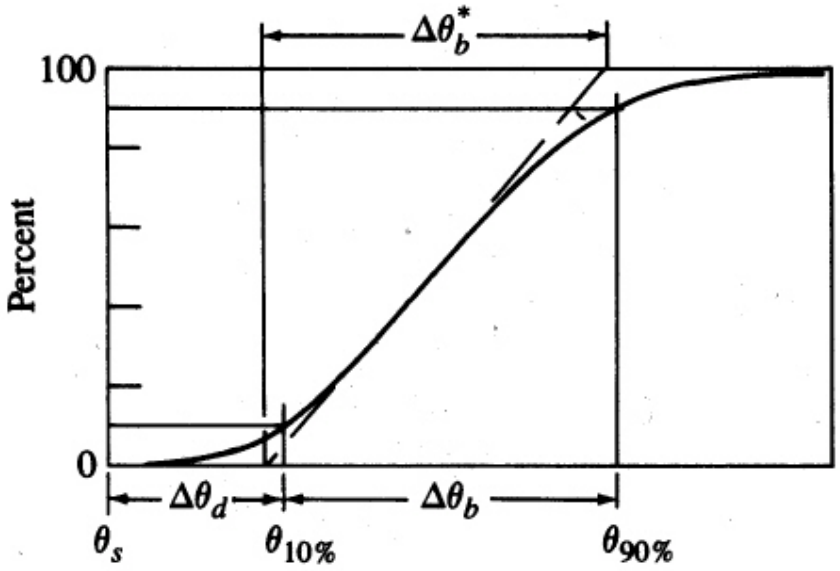

Figure 4: A typical mass fraction burn profile. [25]

More detailed phenomenological combustion models which simulate flame propagation have also been developed. These are used by researchers when more details (spatial resolution) are needed about the combustion process and the user wants mass burn rates being calculated to respond to changes in cylinder flows and geometry. These models assume a flame front profile and based on the mixture chemistry, engine geometry, fluid behavior and transport properties, they simulate flame prorogation. [25] [26] [27]

2.1.4. Heat Transfer Correlation

The high temperature bulk gases in the cylinder lose heat to the cylinder walls. In some cases this energy exchange can be as high as one third of the fuel's chemical energy [28]. Because of the complex nature of the heat transfer problem, empirically

derived correlations are used to calculate overall heat transfer coefficients (h_c). This along with the cylinder temperature calculated from the engine model, heat transfer surface area and wall temperature, which is an estimated value, is used to calculate the heat transferred to the walls. Some of the more popular correlations are given below:

Nusselt (1923): [29]

$$h_c = C_1 P^{0.67} T^{0.33} (1 + 1.24 u_p) \quad (4)$$

Annand (1963): [30]

$$h_c = C_2 L^{-0.3} P^{0.7} T^{-1.0} {u_p}^{0.7} \quad (5)$$

Woschni (1967): [31]

$$h_c = C_3 L^{-0.2} P^{0.8} T^{-0.35} {u_p}^{0.8} \quad (6)$$

Hohenberg (1979): [32]

$$h_c = C_5 L^{-0.2} P^{0.8} T^{-0.4} (1.4 + u_p)^{0.8} V_{inst}^{-0.06} \quad (7)$$

Different correlations perform better compared to others for different operating conditions and different kinds of engines. So, it is important to choose the right for the problem at hand in order to get an accurate representation of the wall heat loss. Details of the use of these correlations can be found elsewhere [25] [28].

2.2. Gas Exchange Modeling

Based on the thermodynamic definition of a system, an engine cycle can be split into two portions: the open portion and the closed portion. As the names suggest, the open portion is the part where the cylinder is treated as a control volume and the closed portion is the part where it is treated as a control mass. The thermodynamic processes during the closed portion are modeled using techniques detailed in the papers cited in the preceding sections. For modeling the open portion gas-dynamics models are required in addition to the thermodynamic models to calculate mass flows in and out of the system.

The simplest approach to model gas exchange is to treat the flows through ports or valves to be one dimensional and isentropic (adiabatic and reversible). In order for the model to produce realistic results an empirically determined correction factor known as the discharge coefficient (C_D) is used to account for non-isentropic effects. The discharge coefficient is defined as the ratio of actual mass flow through an orifice to the ideal mass flow through it for the same upstream and downstream conditions. Equation (8) gives this ratio.

$$C_D = \frac{actual\ mass\ flow\ rate}{ideal\ mass\ flow\ rate} \tag{8}$$

Discharge coefficient values depend on multiple factors including: port geometry, Reynolds number, Mach number and nature of the gas [25]. Empirical results for values of C_D have been published in literature as a function of upstream and downstream pressure ratio [25] [33] [34] [35] [36]. Using the discharge coefficient, port

area, upstream and downstream conditions and gas-dynamics equations for isentropic choked and non-choked flows [25] [37] mass flow rates through the ports (or valves) can be calculated. For these calculations upstream and downstream pressures and temperatures can either be assumed to have an averaged constant value during the engine run or their values can be changing instantaneously with time. The latter can be done either by modeling the complete intake and exhaust apparatus [38] or crank angle resolved experimental results could be used as boundary conditions for the solution.

Once mass flows have been calculated, then by using the first law of thermodynamics with some simplifying assumptions like uniform temperature across the cylinder [39], cylinder pressures during the open portion can be calculated. Mixing during the scavenging process can be modeled using one zone models like the perfect mixing or the perfect displacement models [1] [33] [39]. Using multi-zone models in which the cylinder is divided into multiple zones can also be an option. Some models divide the cylinder into two zones: a mixing zone and a burned gas zone [40] or a mixing zone and a fresh charge zone [41]. Three zone models having mixing, fresh charge and burned gas zones have also been developed [42][43]. Detailed computational fluid dynamics based approaches are also used to develop gas exchange models [44].

2.3. Second Law Analysis

Performing second law analysis on a thermodynamic system provides the researcher an extra degree of resolution into the transfers and capabilities of the system. Exergy utilization behavior maps are a better metric of the efficiency of conversion of

fuel's chemical energy into higher forms of thermal energies, the highest one being shaft work. It also captures the non-recoverable losses accompanying energy exchanges that cause entropy generation. These are called irreversibilies [45] [46]. It wasn't until recently that researchers discovered the benefits of using second law analysis in their investigations. Vast contributions from Caton [47], Van Gerpen and Shapiro [19] and Rokopoulos [48] in the field have brought this analysis technique to the forefront and compelled engine modelers of today to probe exergy performance of their respective engines.

2.3.1. What is Exergy?

Exergy, also sometimes referred to as availability or essergy (essence of energy) quantifies the potentially useful fraction of energy. This useful fraction of energy is either converted to useful work, transferred, or destroyed due to entropy generation (i.e., irreversibilities). Exergy is generally destroyed when gradients within a system, or between a system and its surroundings, are destroyed without doing useful work and the system moves towards a state of thermodynamic equilibrium with the surroundings. This state is referred to as the dead state. Picturing an ideal heat engine like a Carnot engine that is exchanging heat reversibly with two thermal reservoirs and generating work, helps better understand the concept of exergy. A thermal gradient exists between the two reservoirs; the Carnot heat engine is the reversible system that utilizes this gradient to do useful work. The maximum amount of work that can be produced is equal to work produced by this ideal heat engine. Similarly, presence of pressure gradients between

system and surroundings presents an opportunity to produce useful work too. The maximum amount being equal to that, which can be produced by an ideal expansion device like an ideal turbine [49]. So, exergy depends on not only the state of the system but also the environmental condition.

By probing exergy transfers within a thermal system as gradients are being destroyed and the system is moving towards thermodynamic equilibrium, knowledge about the directionality of processes taking place within the system and the associated potential for doing useful work i.e. exergy, is gained. This is a consequence of the second law of thermodynamics. This knowledge regarding equilibrium conditions can be used to identify processes that are thermodynamically the most inefficient and remedial measures can be suggested to minimize the impact of these processes on the thermodynamic performance of the system. [47]

Thermodynamic equilibrium requires the system to be in mechanical, thermal, phase, and chemical equilibria. The dead state for the first three is defined collectively and is called the restricted dead state. Restricted dead state can be defined at temperature, T_o=298.15K and pressure, P_o=100.325kPa [49] [47]. While the system equilibrates to this dead state, the maximum possible work that can be harnessed is the thermo-mechanical exergy. When the system has reached the restricted dead state, there is still potential to extract some more work because of the chemical gradients present between the system and the surrounding. This potential is quantified by the chemical exergy of the contents of the system. The dead state used in the calculations of chemical exergy is known as the true dead state [45]. At this state no chemical, thermal or

mechanical gradients exist between the system and the surrounding. The potential for producing work during the destruction of chemical gradients i.e. chemical exergy is quantified by the following expression:

$$A_{ch} = \sum m_i(\mu_{o,i} - \mu_i^o) \qquad (9)$$

Where $\mu_{o,i}$ and μ_i^o are the chemical potentials of specie i at restricted and true dead states, respectively.

Exergy is an extensive property and unlike most thermodynamic properties, e.g. enthalpy and internal energy, exergy is not necessarily conserved. Exergy is transferred accompanying work, heat transfer and mass flow. In addition to these transfers, just like entropy a fraction of exergy can be destroyed because of irreversibilities in the system. In an ideal system which has no heat transfers i.e. adiabatic and is internally reversible the exergy destroued can be equal to zero, but all real world processes involve some fraction of the exergy being destroyed because of irreversibilities within the system like friction, mixing, combustion, and heat transfer through a finite temperature difference. The exergy of a system (not exergy transfer terms) can either be zero or positive, but it can never be negative. Exergy transfers and destruction are expressed by the following expressions:

$$dA_{work} = (P - P_o)dV \qquad (10)$$

$$dA_{heat} = \delta Q \left(1 - \frac{T_o}{T}\right) \quad (11)$$

$$dA_{mass} = a_{in} m_{in} - a_{out} m_{out} \quad (12)$$

$$\delta A_{destruction} = T_o dS = \delta I \quad (13)$$

Upon performing an exergy balance for all the contents of the cylinder as well as the mass in/out flows, the following expressions are obtained [5] [45] [50]:

$$\frac{dA_{cyl}}{d\theta} = a_{in}\dot{m}_{in} - a_{out}\dot{m}_{out} - \frac{dA_{work}}{d\theta} + \frac{dA_{heat}}{d\theta} + \frac{dA_f}{d\theta} - \frac{\delta I}{\delta\theta} \quad (14)$$

$$\frac{dA_f}{d\theta} = \frac{d(mx)}{d\theta} a_{fch} \quad (15)$$

Here 'A_{cyl}' is the exergy of the contents of the cylinder, 'a_{in}' and 'a_{out}' are the specific flow exergies for incoming and outgoing flows, respectively and 'A_f' is the chemical exergy of the fuel. It is calculated from the specific chemical exergy of the fuel values which are available in literature. The chemical exergy of fuel can be expressed per molar basis as [45] [51]:

$$\bar{a}_{fch} = \bar{g}_f(T_o, P_o) - \{\sum x_p(\bar{\mu}_p^o) - \sum x_r(\bar{\mu}_r^o)\} \quad (16)$$

Here the subscripts ‘p’ and ‘r’ denote products and reactants of a stoichiometric combustion reaction of the fuel, respectively. Like in equation (9) the superscript ‘o’ refers to true dead state. Several simplified forms of equation (16) for use in hydrocarbon combustion is internal combustion engines have been formulated [51] [52] [53].

2.3.2. Exergy Analysis of Engines and Expectations for Literature

Once second law analysis has been performed on the cylinder, the effects of different parameters like engine load, engine speed, burn duration, start of combustion timing etc., on the overall exergy destruction can be evaluated. Two good review papers on second law analysis of internal combustion engines have been written by Caton [47] and Rakopoulos et al. [48].

Typical values for irreversibilities in the engine cylinder for CI four stroke engines operating at full load range from 20-25% of the fuel’s chemical exergy [48]. This value is higher (40% or even higher) for spark ignition engines and CI engines at low loads. The main contributing factor towards this behavior is the relatively lower cylinder temperatures and lower mean effective pressures. No work reporting these values for spark ignited two stroke engines was found during literature review. So, the findings of the investigation ought to shed light on where two stroke engines lie in the percentage exergy utilization spectrum under different operating conditions. These trends are shown in figures 5 and 6.

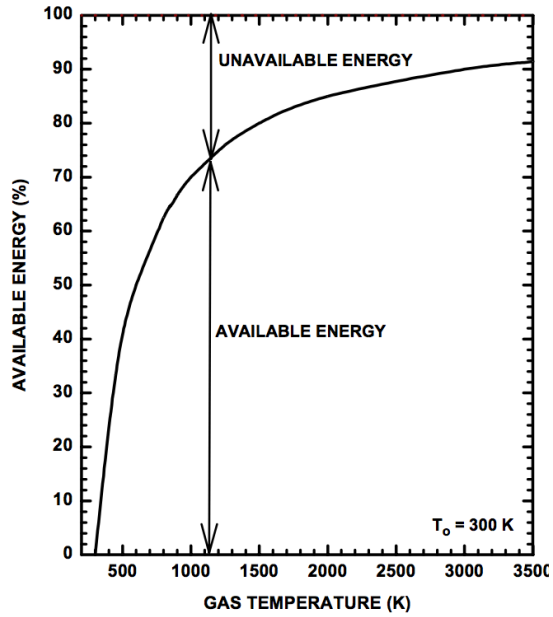

Figure 5: Percentage of energy, which is available to do useful work as a function of gas temperature for an environmental temperature of 300 K. [47]

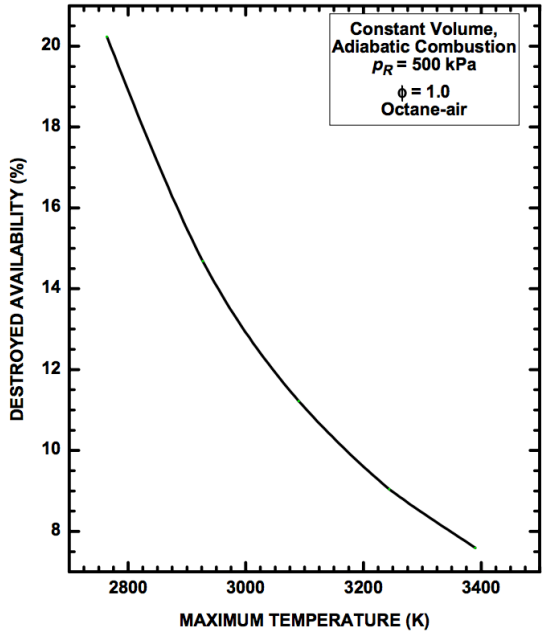

Figure 6: Percentage destroyed during combustion for a constant volume adiabatic system. [54]

Other findings regarding exergy destruction in engines that we know from literature suggest that majority (80%) of exergy destruction during combustion occurs due to heat transfer between the high temperature reacting gases and so far unburned gases [11]. Increasing gas temperature (e.g., increasing engine compression ratio) decreases exergy destruction because the temperature difference between burned gases and unburned gases decreases (utilization temperature approaches supply temperature [45]). Increased gas temperatures, however, increase heat transfer to cylinder walls [48]. The effects of pressure variations during combustion on exergy generation are negligible [54].

2.4. Thermodynamic Property Calculation

In order for all of the aforementioned models/sub-models to perform their respective computations, thermodynamic properties of the mixture at the each crank angle degree have to be known. Property calculators or look-up tables are thus an integral part of any engine simulation package. Such sub-routines rely on empirically determined intensive property values measured at various pressure and temperature values. Extensive properties are calculated by using the mass of respective gas species obtained from gas-exchange and dissociation models.

Some of these properties, like specific internal energy (u), specific enthalpy (h), specific heats (c_p, c_v), are solely functions of temperatures; while some, like specific entropy (s) and specific exergy (a), have temperature as well as pressure dependence. All of these calculations are performed based on the assumption that gases are behaving

ideally, which is a reasonable assumption given the high temperatures observed in engine cylinder.

Numerous calculators can be found from literature, which calculate these properties both for air [55] [56] and fuel [57] [25] [15]. Most of these calculators are actually curve fitted polynomials for the JANAF tables [58], which have thermal properties, as well as equilibrium constants for dissociation reactions tabulated for a range of temperatures and pressures. Using the respective compositions of fuel, air and residual gases calculated from stoichiometric and dissociation sub-routines [59] [25] [15], thermal properties of gaseous mixtures can also be calculated.

3. SIMULATION FRAMEWORK

In the last chapter numerous methods used by engine modelers to model closed and open portions of internal combustion engines as well as exergy transfers within engines were discussed. This chapter builds upon the last chapter and discusses the details of the specific models that have been used in the current study. The sequence followed is the same as last chapter. Closed system modeling is discussed first, followed by open system modeling and exergy analysis.

3.1. Engine and Equipment:

The engine being modeled in the present study is a two-stroke, natural gas fueled, single-cylinder, spark-ignited, naturally aspirated, 9.3 liter, cross-scavenged engine. Engine specifications are detailed in Table 1. A cross sectional view of the engine has been shown in Figures 1 and 2. These engines usually find applications in oil and gas industry where they serve as prime movers for pump jacks or reciprocating natural gas booster compressors. The engine in the lab is coupled with a 50kW, air cooled, eddy current dynamometer and a network of temperature, pressure, angular position/velocity and emissions sensors along with a digital data acquisition system are used to experimentally study the engine's operation at various speeds and loads. Because the current study is not experimental in nature, details of the data acquisition system and dynamometer are not being provided here. The reader is directed towards previous publications from the group [60] [61] to get a more detailed description of the experimental setup. Empirical data obtained from the experiments are used to validate

the thermodynamic models developed in this study. Some of these experimental findings have been reported in a previous investigation by Griffin et al. [44].

Parameter	Units	Value
Bore	mm (in)	215.9 (8.5)
Stroke	mm (in)	254.0 (10)
Displacement	L (in^3)	9.3 (567)
Compression Ratio (effective)	--	6:1
Rated Continuous Power	kW (hp)	29.8 (40)
Rated Speed	RPM	525
Rated Torque	Nm (ft-lbf)	540 (400)
Engine Weight	kg_f (lbf)	2004 (4420)
Flywheel Weight	kg_f (lbf)	680 (1500)

Table 1: Engine specifications

The operating point selected for this study is when the engine is running at full load condition and its rated speed of 525RPM. Full load has been defined as the torque output of the engine at which the engine starts to stall. This operating point was chosen because reliable experimental data was available for validation at this point. Moreover, from previous studies on the engine [61] it is known that the cyclic variations at this point were small (COV of IMEP ≈ 0.02) and the 300 cycle averaged pressure trace was a good representation of individual cycles.

3.2. Solution Methodology

As discussed earlier, the simulation model consists of two primary sub-models, namely the open system and the closed system model, which describe the cylinder conditions during the open and the closed portion of the cycle, respectively. Now, these divisions will be described based on how they've been used in the simulations. The open system of the cycle is the portion between the exhaust port opening (EPO) and the exhaust port closing (EPC), i.e. the portion involving gas exchange. The remaining portion of the cycle is assumed to be closed with no mass transfers. The gases trapped within the cylinder after EPC are compressed, combusted, and expanded during the closed portion, as illustrated in Figure 7. In Figure 7 the arcs describing the compression and expansion portions of the cycle aren't based on the traditional definitions of compression and expansion i.e. decrease and increase in volume, respectively. The boundaries have, in fact, been defined based on the starting and ending points of compression, combustion and expansion subroutines used in the program. Based on the conventional definitions, compression would be extended beyond the start of combustion and continue until TDC. Similarly, expansion would commence from TDC rather than the end of combustion point.

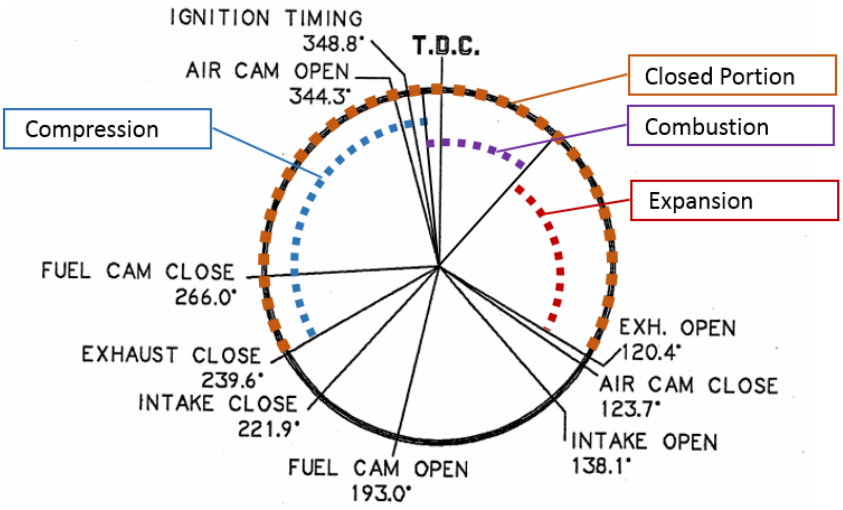

Figure 7: Port timing diagram for the engine under study identifying the open and closed parts of the cycle.

The two main sub-models constituting the basic framework of the program, i.e. closed and open portion sub-models, work in a loop iteratively until convergence is achieved. The flow diagram (Figure 8) illustrates this interaction. The loop starts with an initially guessed value for cylinder temperature and pressure at the start of the closed portion (EPC), the closed portion simulation runs using these initial conditions and computes temperature and pressure maps for angles between EPC and EPO. The mass in the cylinder remains constant during this region, as there is no gas exchange. It is calculated using the ideal gas law. Next, the values of mass, temperature and pressure at the end of the closed portion of the system are provided to the open portion simulation, which runs through the open portion of the cycle and computes properties for the remaining angle (EPO to EPC).

Now, all 360^{o}, i.e. one engine cycle, have been simulated. In order to verify whether the simulated pressure trace is 'good' or not, it is compared against the experimental

pressure trace. This is done by comparing the r^2 values of the simulated and experimental curves. If this value is greater than 0.99, it means the simulated results are acceptable and the simulation can proceed to the second law analysis. If not, then the initially guessed T and P are modified to improve the matching. This is done recursively until a good match is obtained. The iterative changes in T_{guess} and P_{guess} are directed by the difference between simulated indicated mean effective pressure (IMEP) and experimental IMEP. IMEP is a cycle averaged pressure and is a useful metric to compare two pressure curves.

$$IMEP = \frac{W_{cycel,indicated}}{V_d} = \frac{\int_{V_{0^o}}^{V_{360^o}} pdV}{V_d} \qquad (17)$$

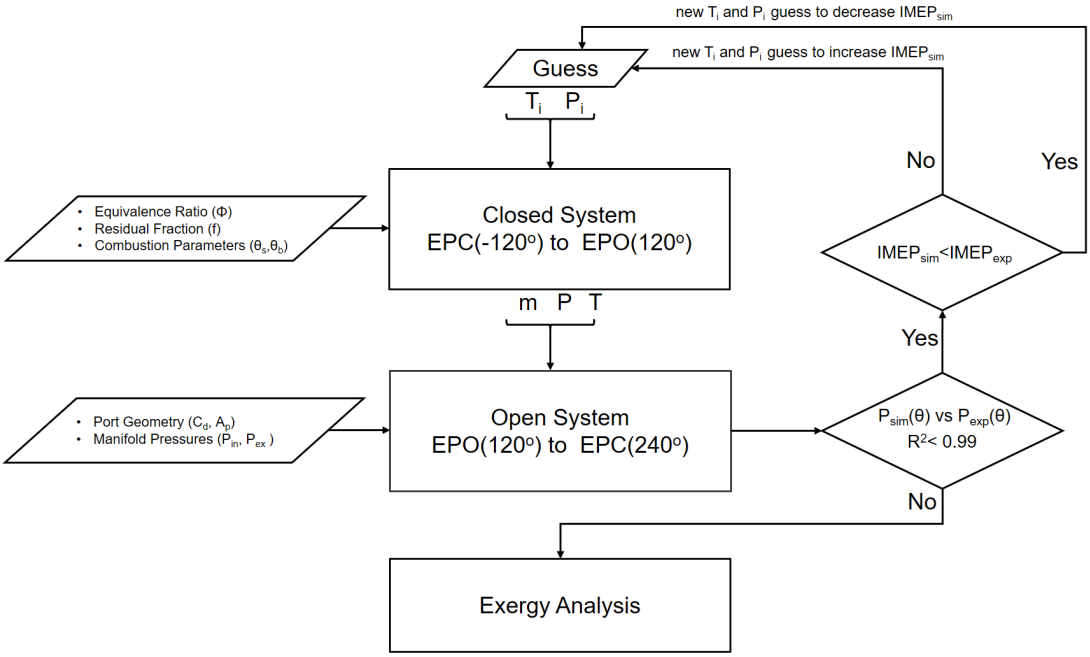

Figure 8: Interaction between open and closed cycle models.

Once an engine model describing cylinder gas properties with respect to engine crank angle exists, numerous other sub-models (e.g. emissions models and exergy models) can be linked to the main model to study desired parameters. In this study, the engine model is linked to a second law analysis sub-model, which studies exergy destruction in the cylinder. These models are discussed in detail in the following sections.

3.3. Closed System Model

The closed system model is developed from the application of the law of conservation of energy applied to a mixture of air and methane (to represent natural gas) being compressed, combusted and expanded in a closed system with varying volume**.** The purpose of this part of the model is to provide initial conditions to the open system portion of the model as illustrated in Figure 7. The model has no spatial resolution (0-D) and has two zones: a burned zone and an unburned zone. It is in fact an adaptation of a model developed by Ferguson [15] for four stroke engines. This model after being modified for two stroke engines is used here to model the closed portion of the engine.

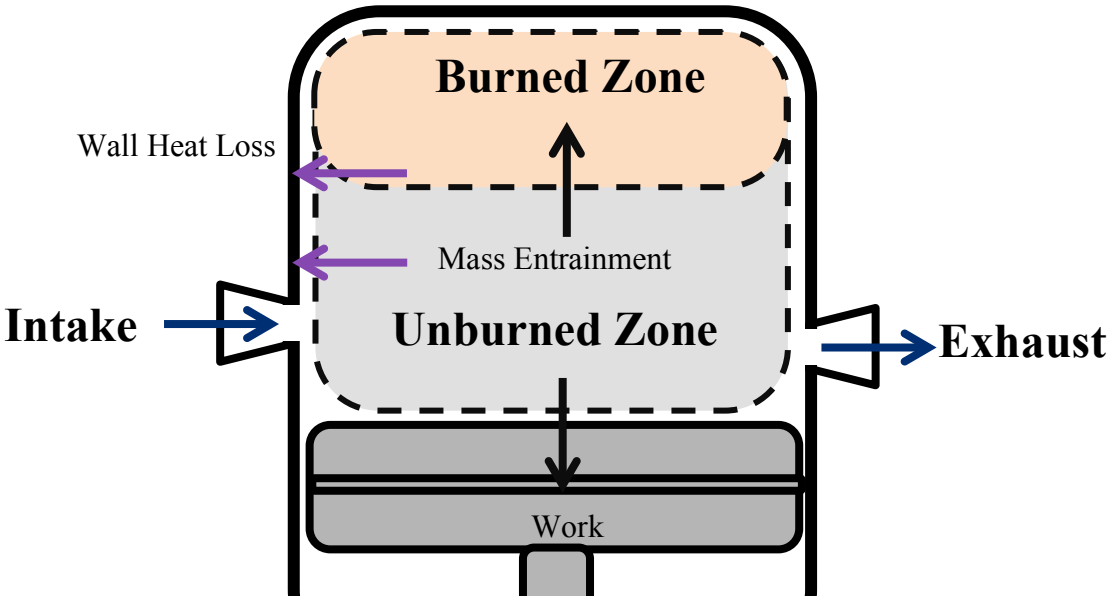

Figure 9: Schematic diagram of the two-zone model.

Figure 9 illustrates the two zones modeled in this simulation. The burned zone consists of high temperature gases which have undergone combustion and the unburned zone comprises of the fresh fuel air mixture. The composition of this mixture is fixed by the equivalence ratio and residual fraction. Initially (right after EPC) the whole chamber comprises of the unburned zone. At a defined start of combustion time, combustion initiates and a burned zone is generated. With time, the burned zone grows and consumes the unburned zone. The details of the combustion model, which dictates the migration of mass from the unburned zone into the burned zone, are discussed in a subsequent section. Chemical energy is released by the fuel as it burns. A fraction of this energy is used to produce pressure-volume work and a fraction is lost to the cylinder

walls through heat transfer. The wall heat transfer is modeled using empirical heat transfer correlations that have been tuned to match experimental data.

The main governing equation for the model is a differential form of the first law applied to both the zones assuming that the gases behave ideally. The equation when written on a crank angle basis assumes the form:

$$m\frac{du}{d\theta} + u\frac{dm}{d\theta} = \frac{\delta Q}{d\theta} - P\frac{dV}{d\theta} - \frac{\dot{m}_l h_l}{\omega} \tag{18}$$

The last term in this expression accounts for the energy loss accompanying blow by fluid losses across the piston rings. It is described by a blow-by constant '*C'* that depends on the piston ring design. In the current study, blow-by losses are ignored.

This equation is simplified to an expression (equation 19 [15]) that is easy to work using numerical solvers. Inputs needed to solve this expression are provided by various subroutines.

$$\frac{dP}{d\theta} = \frac{A+B+C}{D+E} \tag{19}$$

$$A = \frac{1}{m}\left(\frac{dV}{d\theta} + \frac{VC}{\omega}\right) \tag{19a}$$

$$B = h\frac{\frac{\pi b^2}{2} + \frac{4V}{b}}{\omega m}\left[\frac{v_b}{c_{pb}}\frac{dlnv_b}{dlnT_b}\, x^{\frac{1}{2}}\frac{T_b - T_w}{T_b} + \frac{v_u}{c_{pu}}\frac{dlnv_u}{dlnT_u}\, x^{\frac{1}{2}}\frac{T_u - T_w}{T_u}\right] \tag{19b}$$

$$C = -(v_b - v_u)\frac{dx}{d\theta} - v_b \frac{dlnv_b}{dlnT_b}\frac{h_u - h_b}{c_{pb}T_b}\left[\frac{dx}{d\theta} - \frac{(x-x^2)C}{\omega}\right] \quad (19c)$$

$$D = x\left[\frac{v_b^2}{c_{pb}T_b}\left(\frac{dlnv_b}{dlnT_b}\right)^2 + \frac{v_b}{P}\frac{dlnv_b}{dlnP}\right] \quad (19d)$$

$$E = (1-x)\left[\frac{v_u^2}{c_{pu}T_u}\left(\frac{dlnv_u}{dlnT_u}\right)^2 + \frac{v_u}{P}\frac{dlnv_u}{dlnP}\right] \quad (19e)$$

Here the subscript 'b' stands for burned and 'u' stands for unburned. 'V' is the total volume of the cylinder, 'v' is the specific volume, 'T' is the gas temperature, 'P' is the gas pressure, 'x' is mass fraction burned, 'c_p' is the constant pressure specific heat, 'ω' is the angular velocity of the crank shaft, 'h' is specific enthalpy and 'b' is the engine bore. The following sub-routines are called during the simulation run to provide the closed system model all the necessary parameters required to solve equation 19.

3.3.1. Fuel, Air and Residual Gas Property Data Subroutine:

Thermodynamic property data for air (79% N_2, 21% O_2), fuel (CH_4) and residual gas mixture is calculated from the curve fitted JANAF polynomials for respective properties. Three such polynomials for constant pressure specific heat, specific enthalpy and specific entropy (at P_o) are given in equations 20, 21 and 22. The coefficients 'a1' to 'a7' have been obtained from Gordon and McBride's [55] publication for the respective gases.

$$\frac{c_p}{R} = a_1 + a_2T + a_3T^2 + a_4T^3 + a_5T^4 \quad (20)$$

$$\frac{h}{R} = a_1 + \frac{a_2 T}{2} + \frac{a_3 T^2}{3} + \frac{a_4 T^3}{4} + \frac{a_5 T^4}{5} + \frac{a_6}{T} \qquad (21)$$

$$\frac{s^o}{R} = a_1 lnT + a_2 T + \frac{a_3 T^2}{2} + \frac{a_4 T^3}{3} + \frac{a_5 T^4}{4} + a_7 \qquad (22)$$

These property values are used in calculations in the models discussed in the following sections.

3.3.2. Equilibrium Combustion Products Subroutine:

In order to account for the chemical dissociation of various mixture components into other species, particularly at high temperatures, the following six dissociation reactions are considered:

$$\frac{1}{2} H_2 \rightleftharpoons H$$

$$\frac{1}{2} O_2 \rightleftharpoons O$$

$$\frac{1}{2} H_2 + \frac{1}{2} O_2 \rightleftharpoons OH$$

$$\frac{1}{2} N_2 + \frac{1}{2} O_2 \rightleftharpoons NO$$

$$H_2 + \frac{1}{2} O_2 \rightleftharpoons H_2 O$$

$$CO + \frac{1}{2} O_2 \rightleftharpoons CO_2$$

Olikara and Borman's [59] curve fitted polynomial coefficients for JANAF data tables are used to calculate the equilibrium constants for these reactions using the expression:

$$logK_p = A\ ln\left(\frac{T}{1000}\right) + \frac{B}{T} + C + DT + ET^2 \qquad (23)$$

The equilibrium constants along with atom balance equations enable us to compute the molar concentrations of all the components present in the gas mixture, and thus using Gordon and McBride's thermodynamic property correlations discussed earlier, we calculate the properties of the equilibrium combustion products being generated by the overall reaction:

$$CH_4 + \frac{a_s}{\emptyset}(O_2 + 3.76N_2) \rightarrow v_1CO_2 + v_2H_2O + v_3N_2 + v_4O_2 + v_5CO + v_6H_2 + v_7H + v_8O + v_9OH + v_{10}NO$$

Where 'a_s' is the stoichiometric number of moles of air required to completely burn one mole of fuel. 'Φ' is the equivalence ratio and 'v_i's are the molar coefficients of the products.

Input Arguments: P, T, Φ

Output Arguments: h, u, v, s ,y_{CO2}, y_{H2O}, y_{N2}, y_{O2}, y_{CO}, y_{H2}, y_H, y_O, y_{OH}, y_{NO}, c_p.

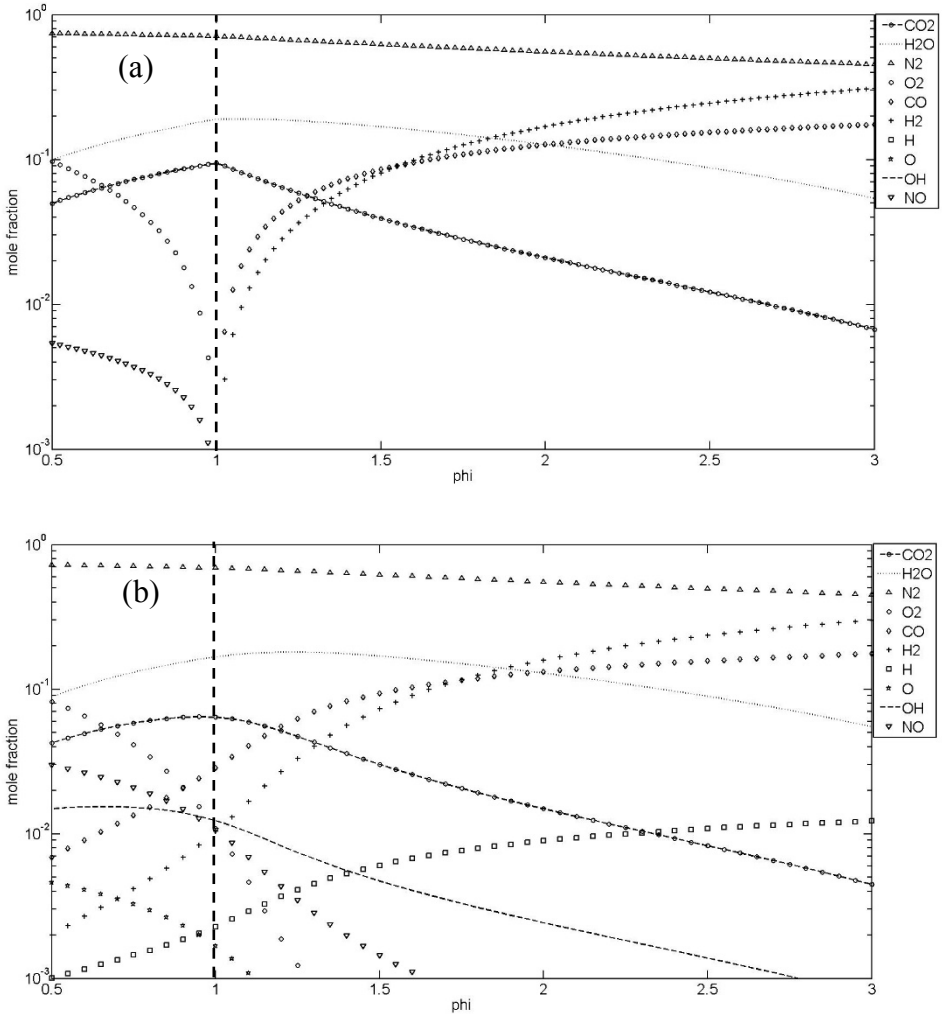

Figure 10: Equilibrium combustion product concentrations at different equivalence ratios at 2000K (a) and 3000K (b) at 50atm.

H, O and OH don't show up in Figure (a) because in the given range their concentrations are negligibly low.

3.3.3. Adiabatic Flame Temperature Subroutine:

Adiabatic flame temperature is the temperature of combustion products that are produced when a fuel reacts with stoichiometric amount of air (oxidizer) in an adiabatic chamber with no shaft work being produced. Energy balance for a control volume reactor with incoming reactants and exiting products reduces to a simplified form which

states that the enthalpies of reactants is equal to the enthalpies of products which are at adiabatic flame temperature. This is the maximum temperature that can be attained by a given fuel upon combustion. An adiabatic flame temperature calculating routine is used to provide an initial temperature for the burned zone at the start of combustion. This is done by equating the enthalpies of the combustion products with the enthalpies of the unburned mixture. These enthalpy values are provided by the fuel, air and residual gas property, and equilibrium combustion products subroutines.

3.3.4. Mass Fraction Burned Subroutine:

The mass fraction burned 'x' is calculated as a function of the crank angle degree by using a Wiebe function (Equation 24). The start and end of combustion are estimated from experimental mass fraction burned profiles at the 1% and 99% mass burnt points. Using these estimates, the start of combustion 'Θ_s' and burn duration 'Θ_b' along with the Wiebe parameters 'a' and 'n' were tuned in the mass burning law until a reasonably accurate match was obtained with the experimental results.

$$x = 1 - \exp\left\{-a\left(\frac{(\theta-\theta_s)^n}{\theta_b}\right)\right\} \qquad (24)$$

3.3.5. Wall Heat Transfer Subroutine:

The correlations developed by Woschni [24] are used to calculate the heat transfer to the wall from each zone. Respective temperatures for each zone and an approximate wall temperature are used in these calculations.

3.4. Open System Model

This part of the model provides initial conditions of mass, pressure and temperature at the start of the gas exchange portion of the cycle, i.e. EPO, by the closed system model. The calculations in the closed portion model were initialized by a guessed value in the first run and by calculated values in successive iterations until convergence was achieved. This is illustrated in Figure 7. The open system model, consequently calculates the cylinder's thermodynamic properties for the crank angle degrees between EPO and EPC. This is the part where gas exchange is taking place. Initially there is only outflow as the intake port doesn't open until 18CAD after the start of EP opening. This is followed by a portion of simultaneous in and out flows (scavenging) and finally after IPC again a portion of only exhaust flow till EPC. Figure 7 diagrammatically details these portions.

The cylinder pressure at various crank angle degrees during the open cycle is calculated using the following equation taken from Benson [62]:

$$\frac{dP}{d\theta} = -k\frac{P}{V}\frac{dV}{d\theta} - \frac{a_{out}^2}{V}\left(\frac{dm}{d\theta}\right)_{out} + \frac{a_{in}^2}{V}\left(\frac{dm}{d\theta}\right)_{in} + \frac{\partial Q}{V\,\partial\theta} \qquad (25)$$

This equation is a restatement of the first law of thermodynamics written in a form which is more popular among gas-dynamics models. It can be written in a form similar to equation 19 too, which doesn't include the speed of sound terms 'a' [22].

$$\frac{\mathrm{dP}}{\mathrm{d\theta}} = \frac{\rho}{\frac{\partial \rho}{\partial P}}\left(-\frac{\dot{V}}{V} - \frac{1}{\rho} - \frac{\partial \rho}{\partial \mathrm{T}}\dot{\mathrm{T}} + \frac{\dot{m}}{m}\right) \tag{25a}$$

$$\frac{\mathrm{dT}}{\mathrm{d\theta}} = \frac{B}{A}\left[\frac{\dot{m}}{m}\left(1 - \frac{\mathrm{h}}{\mathrm{B}}\right) - \frac{\dot{V}}{V} + \frac{1}{\mathrm{Bm}}\left(\dot{m}_{in}h_{in} - \dot{m}_{out}h_{out} - \frac{\partial \mathrm{Q}}{\partial \theta}\right)\right] \tag{25b}$$

Where:

$$\mathrm{A} = \frac{\partial \mathrm{h}}{\partial \mathrm{T}}\left(\frac{\frac{\partial \rho}{\partial T}}{\frac{\partial \rho}{\partial P}}\right)\left(\frac{1}{\rho} - \frac{\partial h}{\partial P}\right) \tag{25c}$$

$$\mathrm{B} = \left(\frac{1}{\frac{\partial \rho}{\partial P}}\right)\left(1 - \rho\frac{\partial h}{\partial P}\right) \tag{25c}$$

Equation 25 was solved in conjunction with gas dynamics equations 26 and 27 which relate the non-isentropic (real) mass flow rate across an orifice of area 'A_R' with upstream stagnation pressure 'P_o' and downstream static pressure 'P_T' . The term C_D, known as the discharge coefficient, captures all the non-idealities in the flow, which makes the flow deviate from its ideal (isentropic) path. Its value ranges between 0 and 1; and depends on the port geometry, its open area and pressure ratio across it. In this study C_D values as functions of pressure ratio across a port were obtained from published data [4]. For the studied engine's geometry and operating speeds, it was found from CFD analysis of gas flow across the ports that the speeds are small enough to assume that stagnation and static properties are equal [44]. Additionally, it is assumed that there is complete thermal mixing within the cylinder gases, such that the temperature throughout the cylinder is uniform.

$$\frac{\mathrm{dm}}{\mathrm{d\theta}} = \frac{\mathrm{C_D A_R P_o}}{\sqrt{\mathrm{RT_o}}} \left(\frac{\mathrm{P_T}}{\mathrm{P_o}}\right)^{\frac{1}{\mathrm{k}}} \sqrt{\{\frac{2\mathrm{k}}{\mathrm{k-1}} [1 - \left(\frac{\mathrm{P_T}}{\mathrm{P_o}}\right)^{\frac{\mathrm{k-1}}{\mathrm{k}}}]\}} \qquad (26)$$

Another form (equation 27) of the mass flow rate equation (equation 26) was used for the cases when the flow is choked.

$$\frac{dm}{d\theta} = \frac{C_D A_R P_o}{\sqrt{RT_o}} (k)^{\frac{1}{2}} \left\{\frac{2}{k+1}\right\}^{\frac{k+1}{2(k-1)}} \; when \; \frac{P_T}{P_o} \leq \left\{\frac{2}{k+1}\right\}^{\frac{k}{(k-1)}} \qquad (27)$$

Equations 26 and 27 have been derived using the definition of mass flow rate ($\dot{m} = \rho AV$) and isentropic relationships between thermodynamic parameters T and P. The orifice area 'A_R' in Equations (26) and (27) is calculated as a function of engine crankshaft location by a subroutine, which assumes linear port opening and closing. A port opening and closing profile symmetrical about the bottom dead center is generated by this sub-routine, which is an accurate depiction of the engine's port behavior (Figure 11).

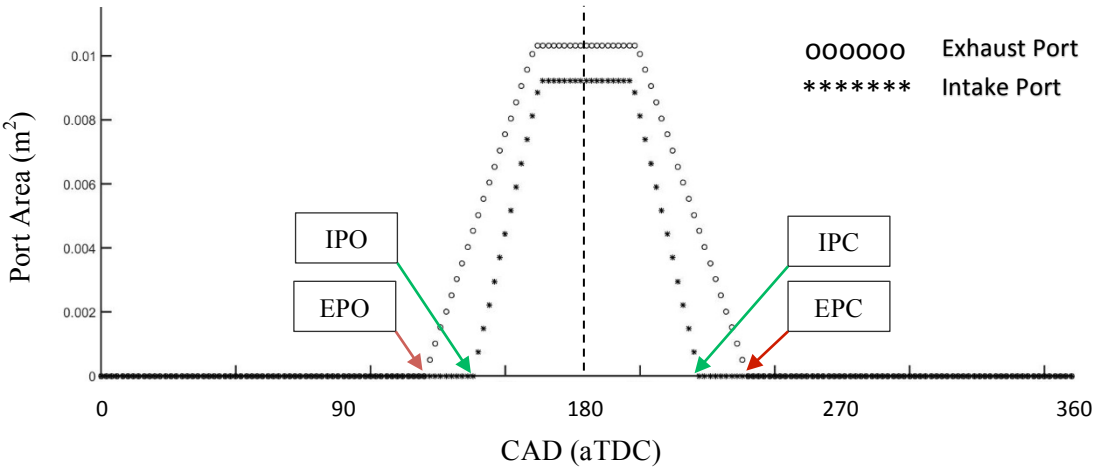

Figure 11: Intake (scavenging) and exhaust port opening profiles.

While applying Equation 26 to the intake process, 'P_T' and 'P_o' are chosen to be the cylinder and stuffing box pressures, respectively. This is inverted for the exhaust process, as illustrated in Figure 12. Since the intake and exhaust systems are not modeled in this study, experimental stuffing box and exhaust manifold pressures were used as boundary conditions in the solution of Equation 25. Back flow exists when 'P_T' is greater than 'P_o'. Suitable checks have been coded into the model to capture these backflows into their respective manifolds.

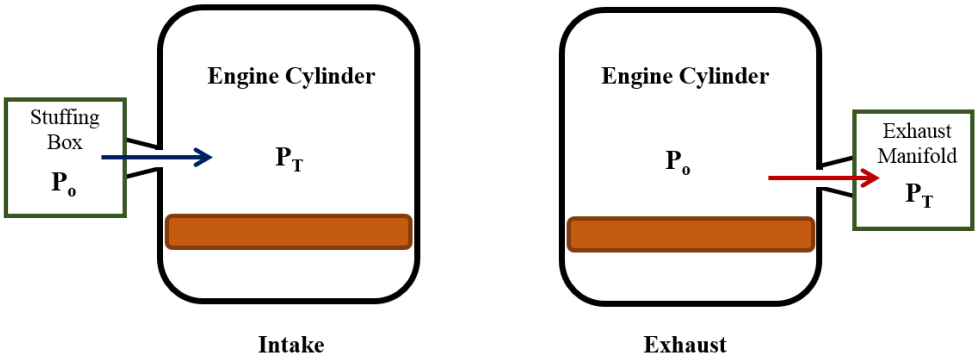

Figure 12: Pressures upstream and downstream of inlet and exhaust ports during gas exchange.

3.4.1. Geometry

The geometry of the engine was modeled using the commonly used kinematic approach where the engine cylinder is assumed to be a perfect cylinder and the volume for various crank angle degrees are calculated. Figure 13 shows the volume profile for the engine being studied. The volume is minimum at 0^o. This is when the piston is at the top dead center and the volume is equal to the clearance volume. The volume is maximum at 180^o when the piston is at the bottom dead center.

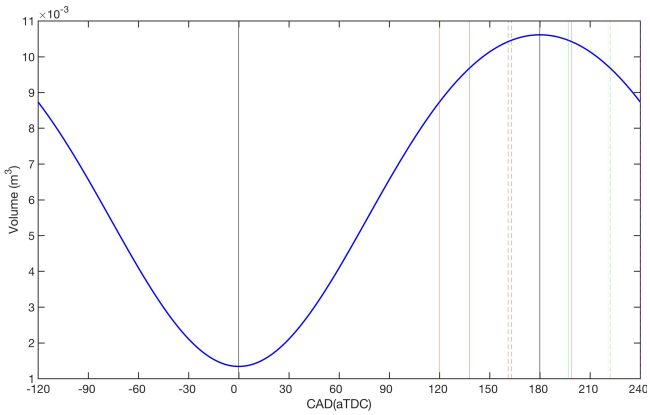

Figure 13: Volume of the engine cylinder for one complete crank angle revolution.

3.5 Exergy Analysis Model

In chapter two numerous approaches to analyze the exergy performance of engines were listed. The current study follows a similar strategy as used by Caton in his second law studies [23][49]. In the previous sections it was discussed how to compute specific entropy values for various gas mixtures at different pressures and temperatures. Using those specific entropy values, cylinder mass and entropy transfer accompanying heat transfer, the total entropy generated by internal irreversibilities within the system is calculated. Mathematically put, this entropy balance is written in the following form:

$$\sigma = S_{end} - S_{start} - S_{in} + S_{out} - S_Q \tag{28}$$

where 'S_{end}' and 'S_{start}' are the total entropies in kJ/K at the end and start of a resolution period, respectively. These can be computed easily since the cylinder temperature and pressure is known at the start and end of all periods between 0^o and 360^o. 'S_{in}' and 'S_{out}' are the total entropies entering and exiting the engine cylinder, respectively. 'S_{in}' and 'S_{out}' are calculated using specific entropies of inlet and outlet gases and the mass flow rates across the engine ports calculated by the gas exchange model. Equation 29 shows these calculations.

$$S_{in} = \int \dot{m}_{in}\, s_{in} d\theta \tag{29a}$$

$$S_{out} = \int \dot{m}_{out}\, s_{out} d\theta \tag{29a}$$

A caveat to be kept in mind while calculating entering and exiting entropy values is that, unlike 's_{end}' and 's_{start}' these values are not necessarily calculated at cylinder temperature and pressure. They are instead calculated at stuffing box conditions for inflows and cylinder conditions for outflows. For backflow through the exhaust port into the cylinder, exhaust manifold conditions are used.

'S_Q' is the entropy transfer into or out of the system accompanying heat transfer. The direction of this transfer is the same as that of the associated heat transfer. This is given by:

$$S_Q = \int \frac{\dot{Q}}{T} d\theta \qquad (30)$$

where 'T' is the temperature of the boundary across which the heat is being transferred. For the two zone model burned zone temperature 'T_b' and unburned zone temperature 'T_u' are used for this calculation.

The rate of entropy generation can be calculated using the rate version of equation 28 given below.

$$\frac{d\sigma}{d\theta} = \frac{dS_{system}}{d\theta} - \dot{S}_{in} + \dot{S}_{out} - \dot{S}_Q \qquad (31)$$

Using equations 28 and 31the exergy destruction (also known as irreversibility) and the exergy destruction rate can be calculated, by multiplying entropy generation with the environment temperature 'T_o'.

$$I = T_o \sigma \tag{32a}$$

$$\dot{I} = T_o \dot{\sigma} \tag{32b}$$

With irreversibility known, exergy of the system can be calculated using the exergy balance equation for a control volume given below. 'B' denotes the total system exergy.

$$I = B_{start} - B_{end} - B_{out} + B_{in} + B_Q - B_W \tag{33a}$$

$$I = -\Delta B_{system} - B_{out} + B_{in} + B_Q - B_W \tag{33b}$$

Like the entropy balance equation 'B_{in}' and 'B_{out}' are the exergies of gases flowing in and out of the cylinder. They are calculated the same way 'S_{in}' and 'S_{out}' are calculated, with the only difference being that specific flow exergies ('b_{in}' and 'b_{out}') are used instead of specific flow entropies ('s_{in}' and 's_{out}'). For a known pressure and temperature flow exergies are calculated using the following expression:

$$b_f = (h - h_o) - T_o(s - s_o) \tag{34}$$

$$B_{in} = \int \dot{m}_{in}\, b_{in} d\theta \tag{35a}$$

$$B_{out} = \int \dot{m}_{out}\, b_{out} d\theta \tag{35b}$$

'B_Q' and 'B_W' are exergy transfers accompanying heat and work transfers. The definition of exergy states that it is the maximum value of potentially useful work

accompanying an energy transfer. It can be concluded from this definition that the exergy transfer accompanying work transfer would be equal to the work since all of the work can potentially be used for doing useful work. Equation 36 mathematically expresses this equality. For energy transferred as heat transfer, however, only a fraction can be used to do useful work. This fraction depends on the temperatures of the system and the environment, which are assumed to behave like the two thermal reservoirs of an ideal heat engine. Equation 37 gives the available fraction of heat transfer.

$$B_W = W \tag{36}$$

$$B_Q = \int (1 - \frac{T_o}{T}) \delta Q \tag{37}$$

With all exergy transfers and destruction known, equation 33 can be used to calculate the exergy of the system for the whole engine cycle. Another way to approach this problem is to calculate exergy of the system using the fundamental mathematical definition of specific exergy given in equation 39 and then using equation 33 to calculate the irreversibility. This can serve as a consistency check.

$$a = (u - u_o) - (-p_o(v - v_o)) - T_o(s - s_o) \tag{39}$$

4. RESULTS

Using the modeling framework discussed in chapter 3 and building upon the knowledge framework provided in chapters 1 and 2, this chapter presents the results of performing first and second law analyses on a two-stroke engine. The energy and exergy utilization of the engine would be probed and compared with that of four stroke engines.

Throughout this chapter many graphs will have vertical lines drawn in the later half (gas exchange portion) of the graphs. These lines represent the timings for various port events and have been described to visualize what, if any, those port events had on the property being investigated. Colored solid lines represent the start of a port event and dotted lines of the same color represent the end of that event. The solid red line at 120^{o} represents the start of exhaust port opening. The dotted red line at 161^{o} represents the end of EPO (i.e., at this point the exhaust port is completely open). The dark green lines do the same for intake port opening. Light green and magenta lines represent the start (solid) and finish (dotted) of intake and exhaust port closure, respectively. Figures 7 and 11 also show these port events. Solid black vertical lines represent the top and bottom dead centers.

4.1. First Law Analysis

In this section results obtained from the application of the first law of thermodynamics on the two-stroke engine are shared. Appropriate forms of the first law are used for the open and closed system portions.

4.1.1. Mass Fraction Burned

The mass fraction burn rate curve calculated from the Weibe function was matched with the S-curve obtained from experimental pressure data using matlab's inbuilt curve fitting toolbox (Figure 14). This was done to get information about the start and end of combustion and using those combustion parameters to tune the Weibe parameters 'a' and 'm'. The results were:

Start of Combustion = -10^{o}

End of Combustion = 40^{o}

Weibe Parameters: a=6.5 and m=1.85.

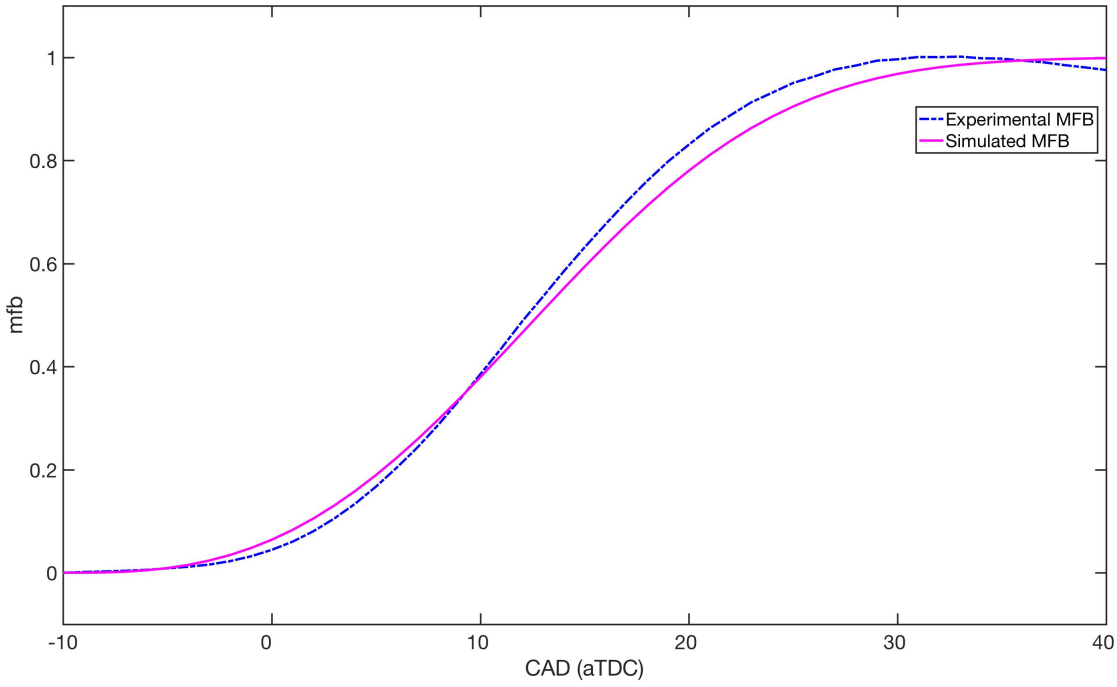

Figure 14: Experimental and simulated (Weibe function) mass fraction burned profiles.

As can be seen from figure 14, the 50% mfb point occurs somewhere around 12° after top dead center, which hints at good combustion phasing. The mass fraction burned calculations were performed using equations 40 and 41 [25], which calculate the rate of heat release fist, and using the ROHR results mfb is calculated. Heat transfer is ignored in these calculations.

$$ROHR = \left(\frac{1}{k-1}\right)\left(kP\frac{dV}{dt} + V\frac{dP}{dt}\right) \tag{40}$$

$$mfb = \frac{(AirFuelRatio+1)ROHR}{m\,(1-r)Q_{LHV}} \tag{41}$$

where 'k' is the ratio of specific heats, 'r' is the residual fraction from last cycle and 'Q_{LHV}' is the lower heating value of the fuel.

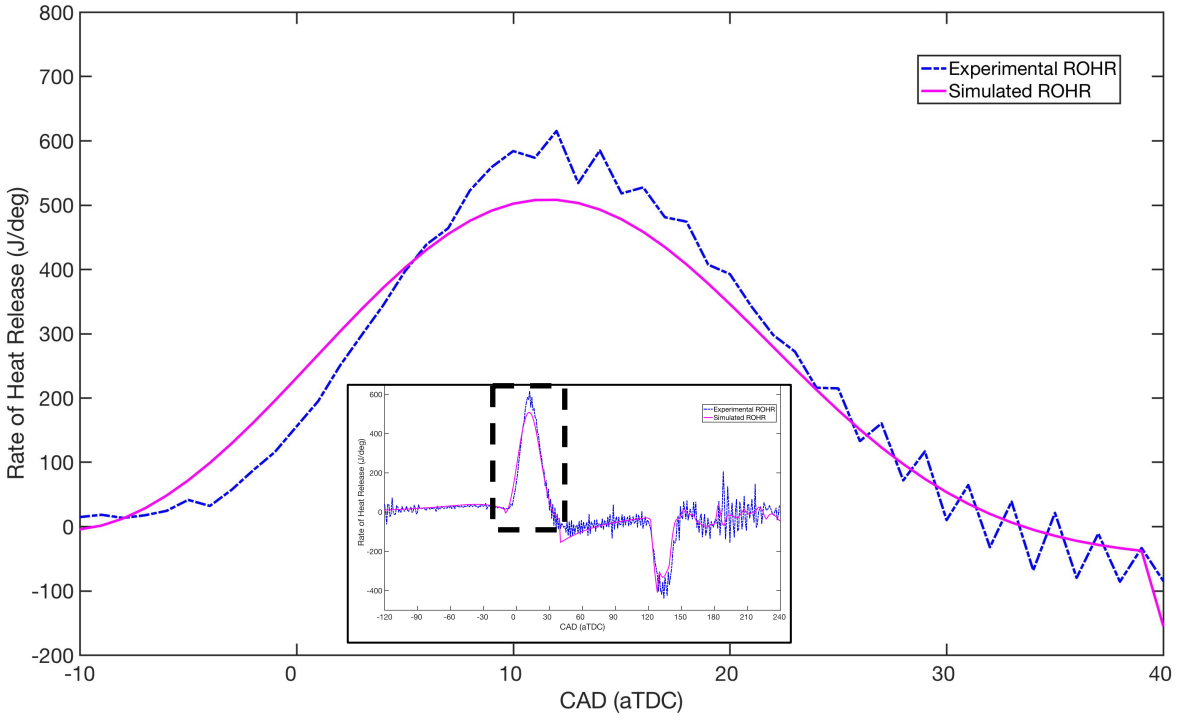

Figure 15: Rate of heat release calculated for experimental and simulated pressures.

Figure 15 shows the rates of heat release in J/deg for experimental pressure data (dotted blue curve). Since only the part of the cycle where combustion is taking place (-10^o to 40^o) is of interest while looking at ROHR only this region has been blown up. The whole cycle can be seen in the insert. The noise in the blue curve is because of the noise in experimentally measured pressures. ROHR calculated from simulated cylinder pressure (pink curve) has also been shown for reference.

4.1.2. Cylinder Pressure

Figure 16 is the final pressure trace obtained after solving equations 19 and 25. The dotted red line is the experimental trace. The solid blue line is the simulated pressure calculated using the closed system model (equation 19) and the black line is pressure calculated using the open system model (equation 25). The simulated results match the experimental results reasonably well. A sharp drop in pressure can be observed at 120^o when the exhaust port starts to open while the intake port is still closed. The expansion process taking place in the cylinder because of downward (towards BDC) motion of the piston also contributes to this drop. All flows are out of the cylinder at this time. Once the intake port starts to open at 138^o, inlet flows counteract the effects of outflows and the pressure stabilizes around atmospheric pressure. When the piston reverses direction at 180^o and starts moving towards TDC, the rise in pressure because of compression is negligible during the gas exchange portion, but once the ports close at 240^o, cylinder pressure starts to rise quite rapidly. This rise becomes even more rapid close to the TDC when combustion starts. Combustion continues until 40^o after TDC but by this time the

pressure has already started to drop because of the counteracting influence of expansion. This steady drop continues until exhaust port opening. At 21^{o} after top dead center peak cylinder pressure of 2343 kPa is observed.

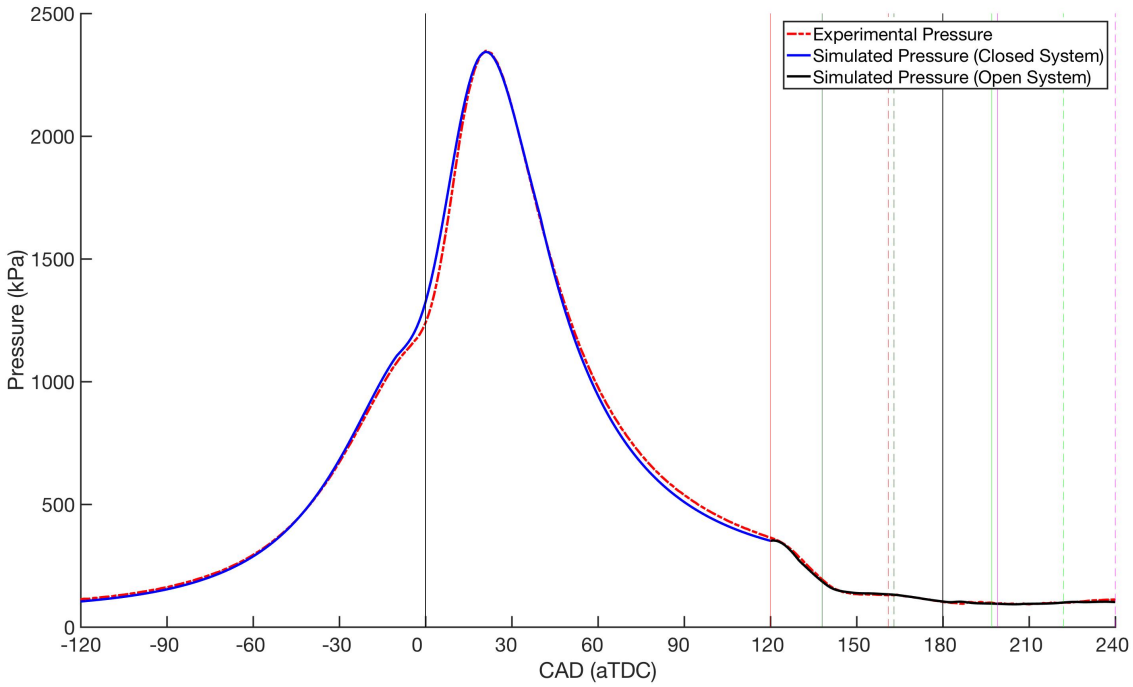

Figure 16: Simulated and experimental cylinder pressures for one cycle.

4.1.3. Cylinder Temperature

Figure 17 shows the temperature of the cylinder gases calculated using the first law of thermodynamics and the ideal gas equation. The dotted pink and blue lines represent the temperatures of the unburned and burned zones, respectively. The solid black line shows the simulated bulk gas temperature. As with pressure, temperature

increases during compression, this increase becomes really rapid once combustion starts and as the piston moves away from TDC, towards BDC, temperature starts to drop because the rate of combustion isn't as rapid anymore and also because of cooling caused by expansion. This decrease in temperature becomes more rapid during the gas exchange portion. Even compression (180^o to 240^o) isn't able to change this trend while gas exchange is taking place. At 30^o after top dead center peak temperature of 2119K is observed.

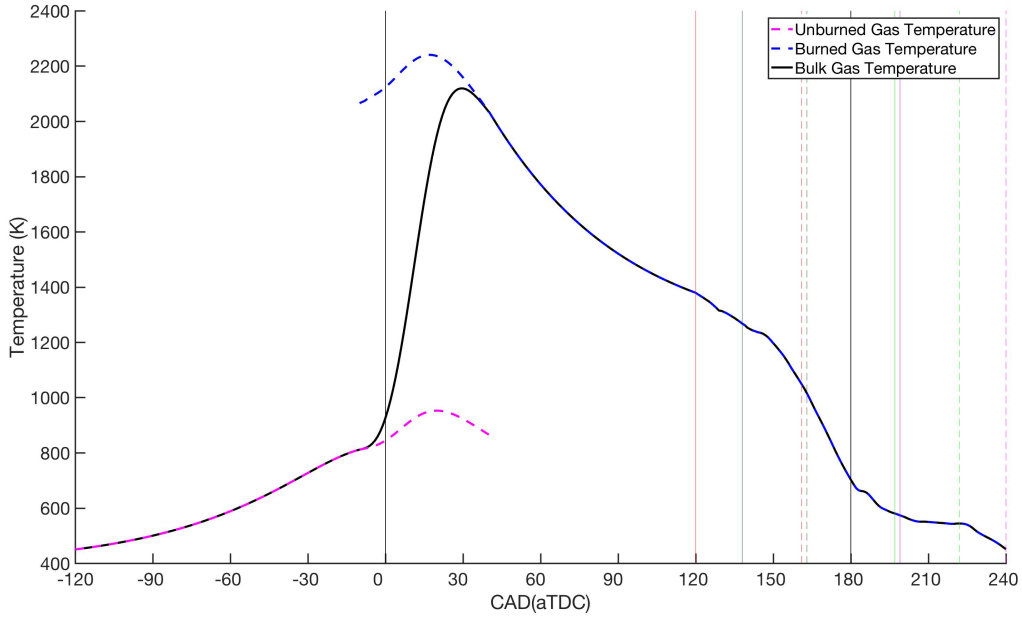

Figure 17: Simulated cylinder temperature for one cycle.

\

4.1.4. Mass Flows

Figure 18(a) shows the rate of mass flow in and out of the cylinder. Positive rates show inflows and negative rates represent outflows. These curves were obtained by solving equations 26 and 27 using experimental stuffing box and exhaust manifold

pressures as boundary conditions. The blue curve is the mass flow rate through the inlet port and the red curve is the flow rate through the exhaust port. Under normal conditions flows though the inlet port are inflows (positive flow rate) and flows through the exhaust port are out flows (negative flow rates). But, there are some instances during the gas exchange processes where backflow through the inlet port into the stuffing box and backflow through the exhaust port into the cylinder take place. For inlet port, this happens whenever the cylinder pressure is higher than the stuffing box pressure and for exhaust port this happens when the exhaust manifold pressure is higher than the cylinder pressure. These flows are also captured by the gas dynamics model and have been shown in Figure 18. Most of these backflows are after 210^{o} when the ports are starting to close.

The experimental stuffing box and exhaust manifold pressures used in the solution of Equations 26 and 27 have been shown in Figure 18(b). The solid blue line shows the pressure of gases in the stuffing box as a function of crank angle degrees. This pressure increases as the piston moves towards the bottom dead center and stuffing box gases are compressed and no fresh air or gas is being inducted into the stuffing box because of positive pressure gradient between the stuffing box and intake manifold. The solid red line shows the exhaust manifold pressure measured experimentally as a function of crank angle degrees. Exhaust pressure fluctuates around 100kPa during the closed portion of the cycle but it shoots up to about 160kPa when the exhaust port opens and high pressure burned gases flow through the exhaust port into the exhaust manifold.

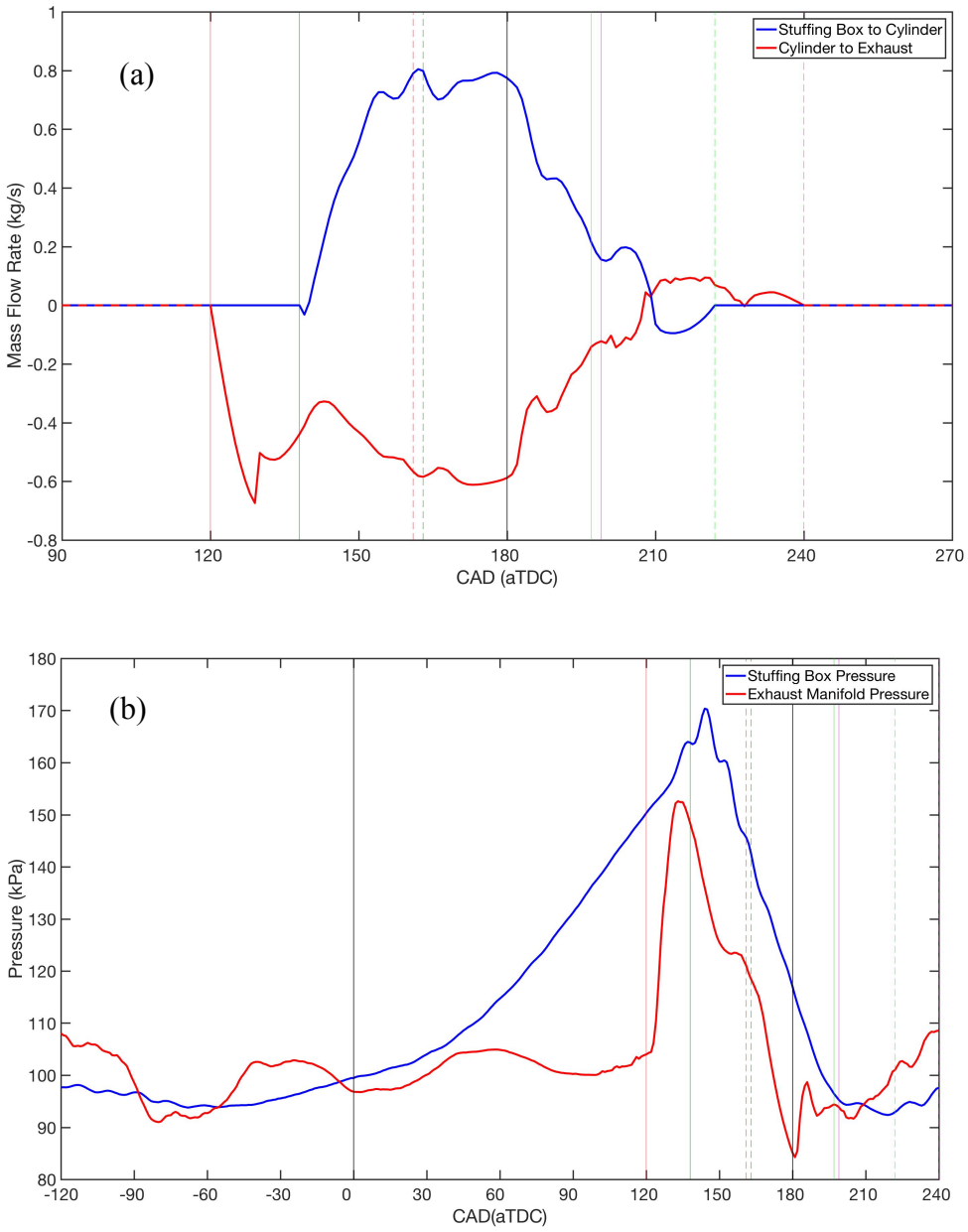

Figure 18: (a) Mass flow rate in and out of the engine cylinder. (b) Experimental stuffing box and exhaust manifold pressure.

The mass flow rate is integrated in order to calculate the total mass in and outflows. The sum of the mass in and out flows gives us the instantaneous mass in the

cylinder. Figure 19 shows the total mass present in the cylinder at any instance. It is observed that initially there is a significant flow out of the cylinder because of the high pressure differential across the exhaust port.

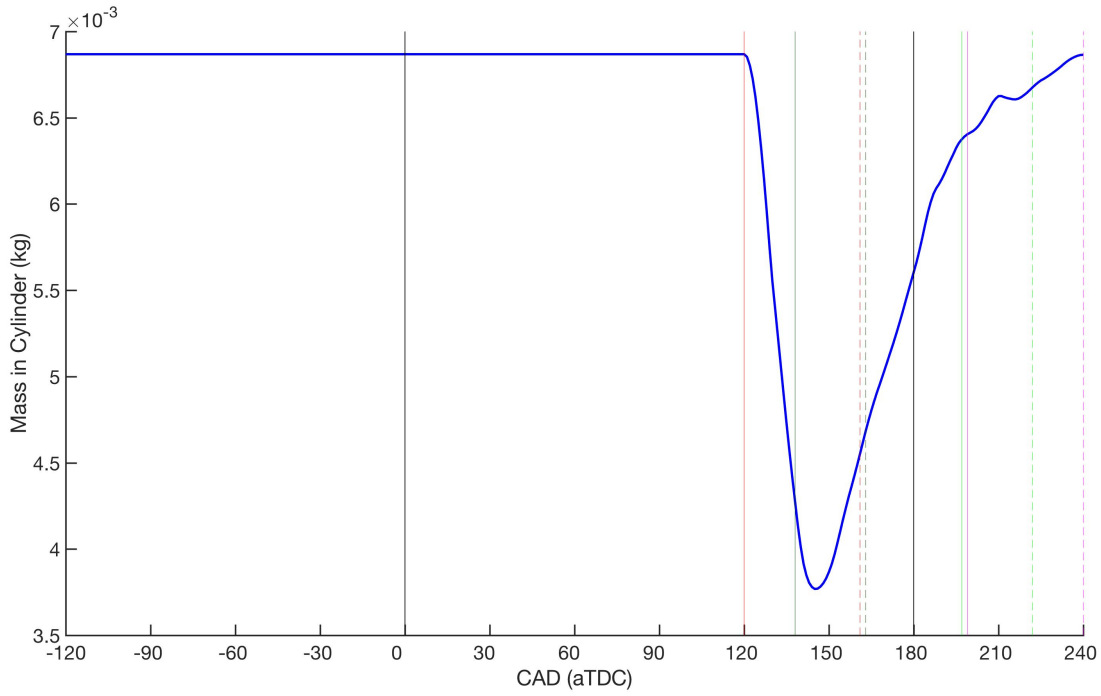

Figure 19: Mass of gases present in the engine cylinder.

When the inlet port opens and gases enter the cylinder from the stuffing box, the total mass in the cylinder starts to stabilize and around IPC it reaches a steady value. This is the mass of the air fuel mixture that would be compressed, combusted and expanded in the closed portion of the next cycle. From the mass inlet and net mass retained curves it is observed that a significant portion of the incoming gas is being exhausted and trapping efficiency, which is a ratio of the amount fresh charge that is

trapped (0.0069kg) in the cylinder after the aspiration processes has ceased to the amount of charge that was supplied (0.0282kg), is around 25%. This number suggests that the gas exchange process is extremely inefficient. In order to have more confidence about the gas exchange performance of the engine specialized studies concentrating on engine scavenging are needed.

4.1.5. Work

The indicated work for an engine is calculated by integrating the instantaneous cylinder pressure over the whole 360^o volume sweep (equation 42). This value does not include the effects of friction. The work which is measured experimentally through a dynamometer incorporates these friction effects and is known as brake work.

$$W_{cycel,indicated} = \int_{V_{0^o}}^{V_{360^o}} PdV \qquad (42)$$

Using the experimental pressure trace and the geometric model, indicated work was calculated for the engine. The results integrated over crank angle degrees are shown in Figure 20. Accumulated work at the end of a cycle is around 4kJ, which is quite close to the rated power value of 29.8kW at 525RPM. This translates to 3.5kJ at 525RPM and 3.6 KJ at 500RPM.

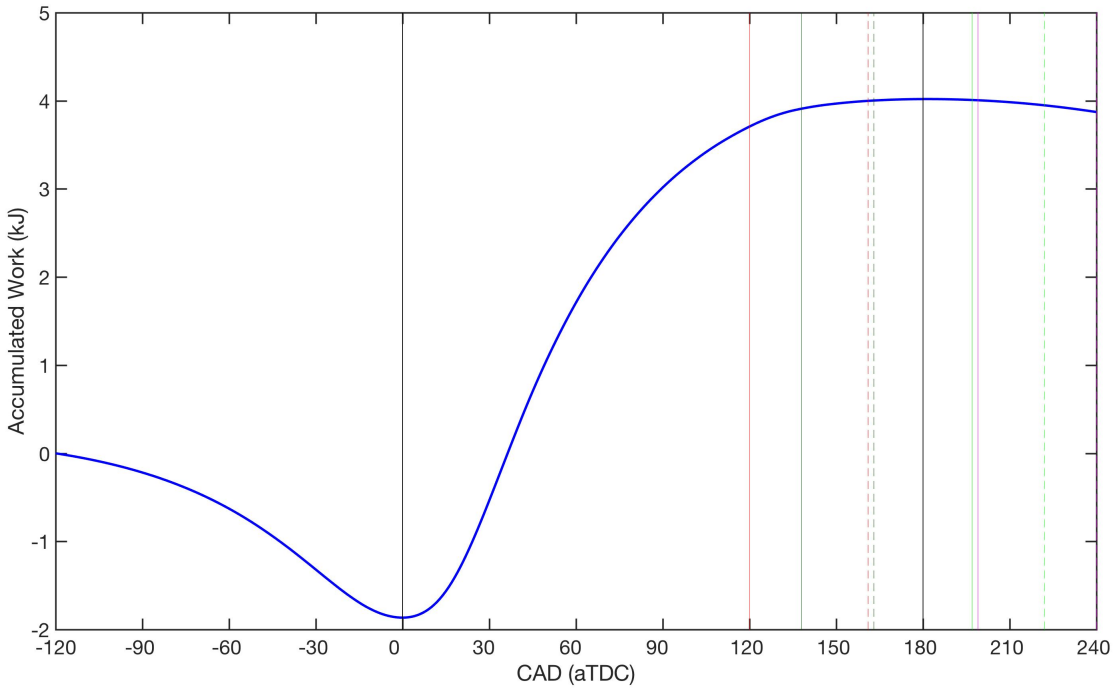

Figure 20: Accumulated work for one complete engine cycle.

Initially work is being inputted to the system during compression i.e. compression work. Work into the system is negative and because of this during the compression accumulated work is negative and decreasing. When the piston changes direction and expansion stoke which is also the power stroke starts, the high-pressure cylinder gases start pushing against the piston to output shaft work. This can be seen in the accumulated work curve as it starts to increase after 0^{o} and continues to do so until 180^{o}, after which it decreases again when expansion starts.

4.1.6. Wall Heat Transfer

Heat loss from the hot cylinder gases to the wall was calculated using the Woschni correlation. Figure 21 shows the accumulated wall heat transfer calculated using a constant wall temperature of 500K. Figure 21 should be analyzed in conjunction with figure 17, which describes the cylinder gas temperature as a function of crank angle. Initially during the compression process when the temperature difference between the wall and cylinder gases is low, there isn't significant heat transfer with the walls. This is why the curve is almost flat until -30^{o}. In fact, if we look closely, there is a slight dip in the curve in the starting portion. This is because at this point the bulk gas temperature is less than the wall temperature and heat is being transferred from the wall to the cylinder gases.

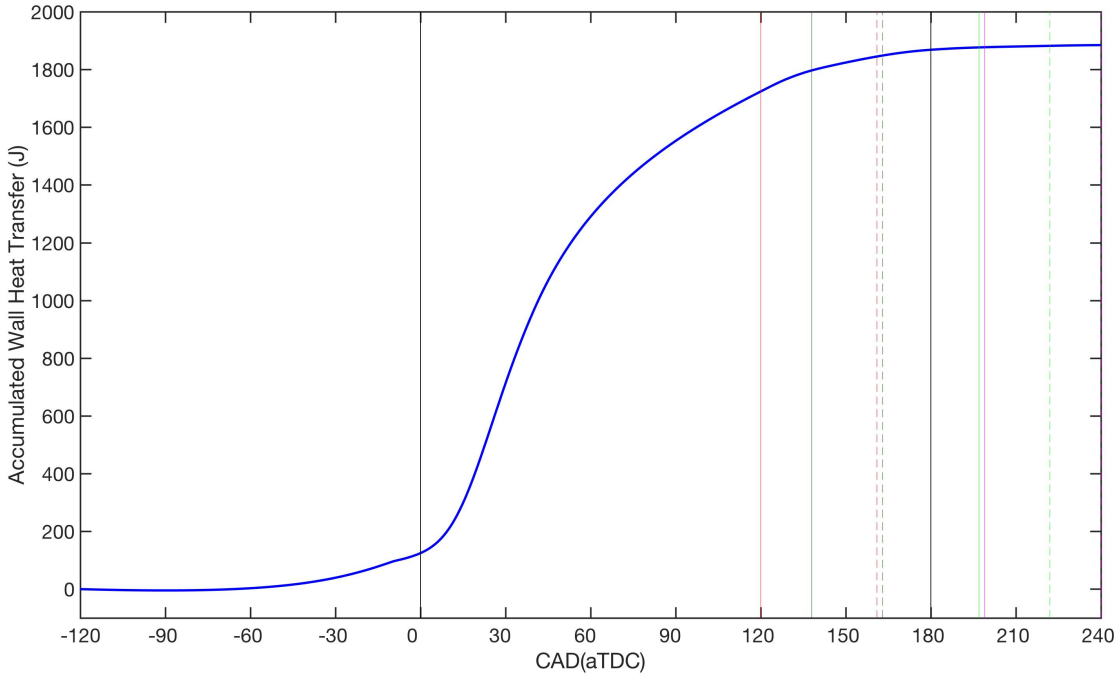

Figure 21: Accumulated wall heat transfer during one complete engine cycle.

The sign convention for heat transfer is opposite to that of work; heat transferred into the system is negative and vice versa. Once the gases start to get hot because of compression and after -10^{o} because of combustion too, wall heat transfer shoots up and this is why the rapid rise in the accumulated heat transfer curve is observed after TDC. This continues till exhaust ports open and gas temperatures drop close to the wall temperature. At this point the accumulated heat transfer curve plateaus.

4.2. Second Law Analysis

As discussed in the previous sections, unlike the first law which treats all forms of energy, be it heat transfer or work, equally, the second law distinguishes between the two based on their quality i.e. their potential to do useful work. Exergy is a tool developed by thermodynamicists to quantify this quality of energy. In this section the results of solving entropy and exergy balance equations listed in chapter 2 and 3 for the engine being studied are shared. It should be noted that the second law results have only been performed on the closed portion of the cycle (-120^{o} to 120^{o}).

After first law analysis has been performed and system properties are known, second law analyses can be carried out on the thermodynamic system using the first law results. The approach being adopted doing so is the one mentioned in section 3.5. To start the analysis entropy values are required for the cycle. Figure 22 shows the cylinder bulk gas temperature as a function of specify entropy. Entropy after a process will include entropy generation, which is a measure of the irreversibility of a process, so it is

expected that maximum entropy rise would be observed during the highly irreversible process of combustion. Results shown in figure 22 agree with this intuitive guess.

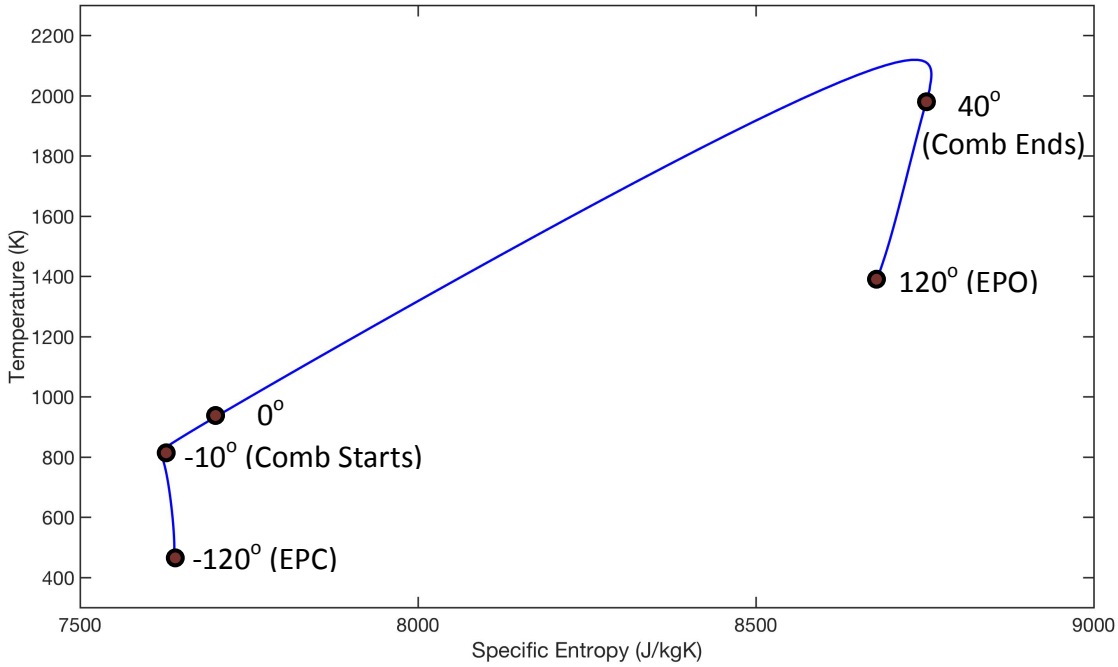

Figure 22: Temperature-Specific entropy diagram for the current operating condition.

Prior to the start of combustion the process from EPC to SOC is almost isentropic as the gas temperature rises. The specific entropy, in fact, increases during the initial part of this process because of entropy added to the system through heat transfer to the cylinder gases from the wall. Later on specific entropy decreases as the direction of this heat transfer reverses because of rise in gas temperature after compression.

Once combustion starts the cylinder gas temperatures increase drastically which is why the specific entropy rises rapidly during this phase. This rise reflects the increase

in system's internal irreversibilities because of combustion. Specific entropy peaks around 30^{o}, which is the point of peak temperature. As combustion stops and expansion causes gas temperatures to cool, entropy decreases slightly and continues to do so till EPO. Even though specific entropy values for the open portion of the cycle haven't been calculated it can be hypothesized based on our knowledge of cylinder temperature that the entropy would decrease rapidly during this phase.

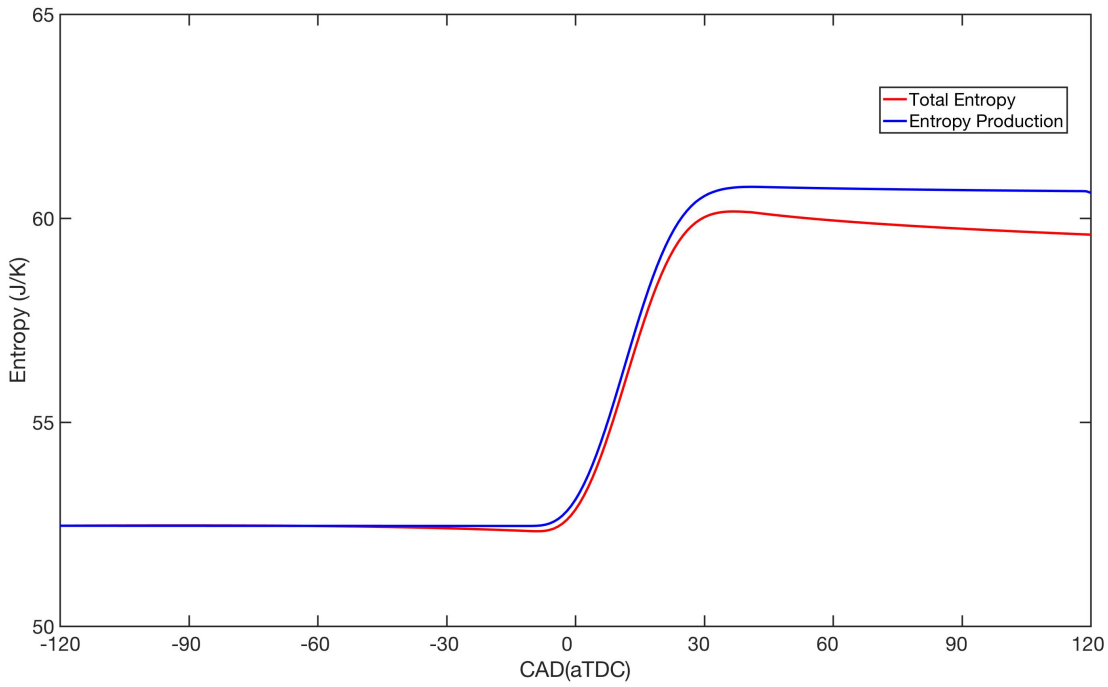

Figure 23: Total entropy as a function of crank angle for the current operating condition.

The same results regarding entropy behavior can also be seen from figure 23, which shows the total system entropy as a function of crank angle degrees. The total entropy remains virtually unchanged prior to the start of combustion and then it rises

rapidly during combustion. Next, it decreases because of cooling of cylinder gases. The initial pre-combustion decrease in entropy because of heat transfer from cylinder gases to the wall can also be observed in figure 23. The blue line represents the entropy generation within the system and as expected entropy is generated during the highly irreversible combustion process. The difference between the red and the blue lines is the entropy transfer due to heat transfer.

With the specific entropy (figure 22) and internal energy (figure 24) of the system known, the specific exergy of the system can be computed. Figure 25 shows the specific exergy as a function of crank angle degrees. After EPO the specific exergy increases slightly because of compression work, which is being done on the system. Thus, increasing the system's potential to do work. After the start of combustion, specific exergy decreases because of destruction and outflows of potential work opportunities in the shape of combustion irreversibilities, heat transfer to the walls and expansion work. The specific exergy continues to decrease even after combustion has ended and temperature starts to decrease because work and heat transfer are still removing exploitable energy out of the system.

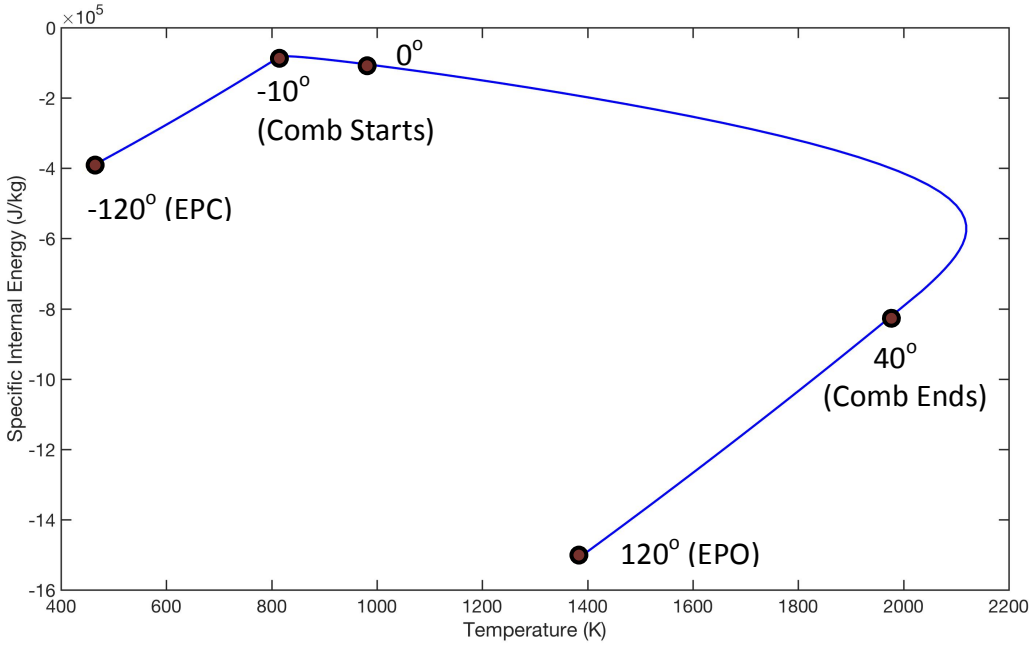

Figure 24: Specific internal energy as a function of bulk gas temperature.

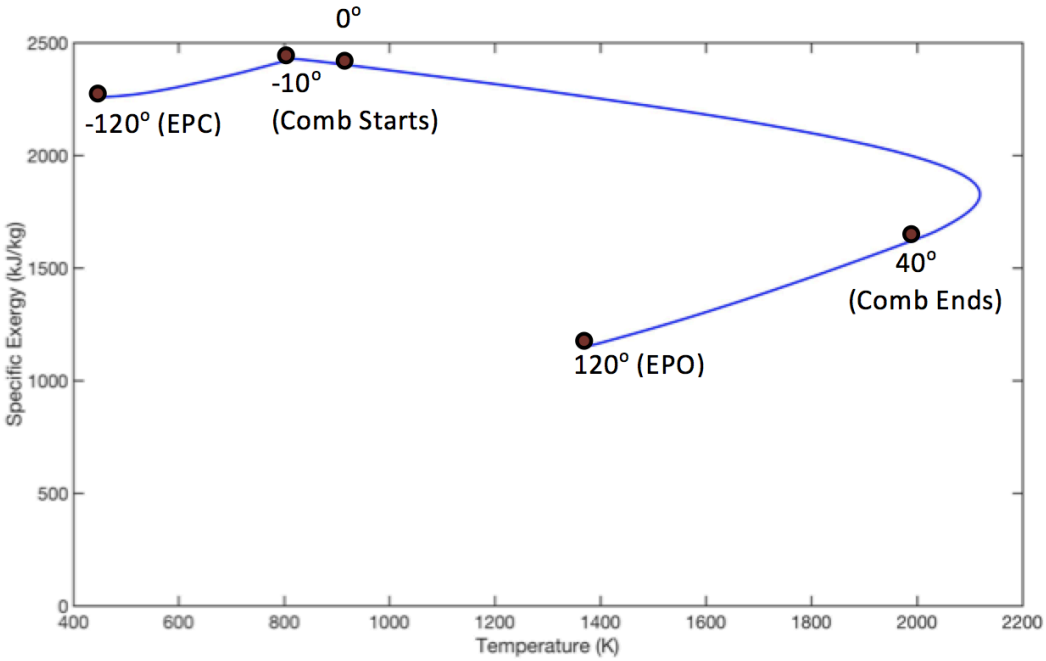

Figure 25: Specific exergy as a function of bulk gas temperature.

Knowing the irreversibility (exergy destruction), work and heat transfer for the cycle; exergy balance equations can be used to calculate the total system exergy as a function of crank angle. Figure 26 shows the evolution of total system exergy, as well that of exergy destruction and exergy transfers with heat transfer and work. At the start of the cycle, right after exhaust port closure, the cylinder is full of fresh charge. Knowing the equivalence ratio, residual fraction (if any) and mass of the trapped charge, mass of fresh fuel can be calculated. If the chemical exergy per unit mass of the fuel is known the total available chemical exergy of the cylinder gases can be calculated. Simpson and Lutz's work on exergy analysis [63] was used to obtain chemical exergy and lower heating value values for methane. These values are as follows:

$$LHV=50.01 MJ/kg$$

$$a_f = 51.72 MJ/kg$$

These values are consistent with the ratio of specific exergy to heating value mentioned by Kotas [64] for methane. According to Kotas this ratio should be:

$$1.04 \pm 0.5\%.$$

In figure 26 the solid magenta line represents the total exergy of the system. During the compression process, exergy of the system increases because of compression work. During the combustion and expansion stages the total system exergy decreases

because of irreversibilities associated with combustion and heat transfer to the walls; and expansion work that is extracted form the engine. The exergy at the end of the closed cycle i.e. at EPO, is exhausted to the environment.

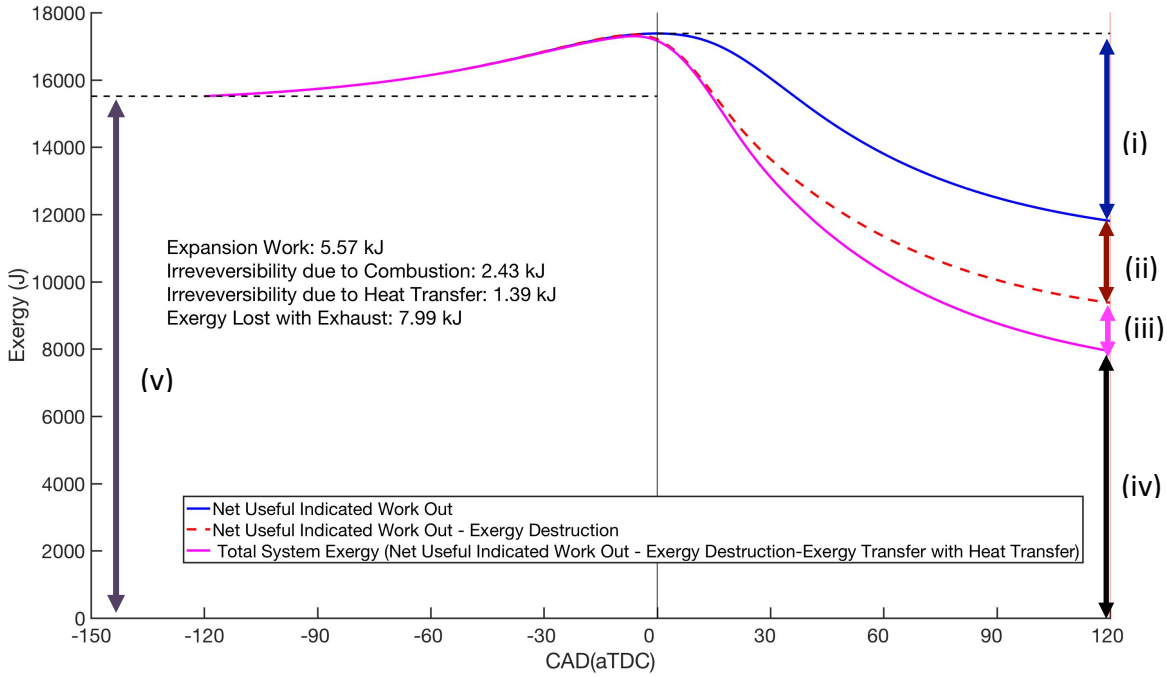

Figure 26: Cylinder charge exergy vs. crank angle for one complete engine cycle at the current operating conditions. (i: expansion work, ii: irreversibility due to combustion, iii: irreversibility due to heat transfer, iv: exergy lost to exhaust, v: chemical exergy of the fuel)

Figures 27 and 28 compare the energy and exergy utilization distribution for the case being studied. Figure 27 compares the absolute amounts in kJ while figure 28 compares the percentage distribution. The amount of expansion work is same for both energy and exergy analysis because 100% of expansion work is available to be *converted into useful work*. The energy lost due to heat transfer is larger than the exergy lost due to heat transfer. This is because a fraction of the energy associated with heat

transfer has the potential of being converted into useful work. Less exergy (8kJ) is released into the atmosphere with exhaust gases as compared to the energy (9.6 kJ) exhausted. This difference shows that the potential for harnessing energy from the exhaust is less than what the first law analysis results would have the reader believe. Lastly, there is a fraction of the exergy, which is destroyed because of irreversibilities while all of the energy is conserved.

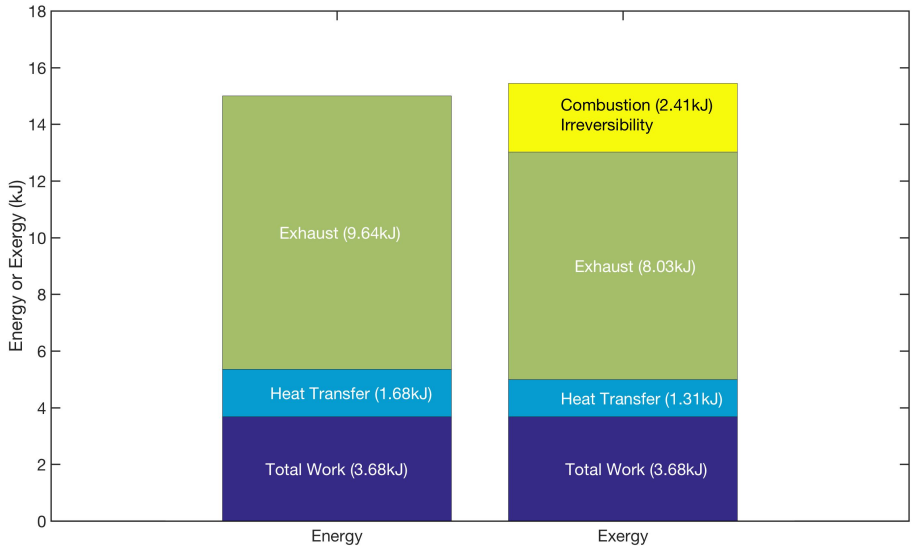

Figure 27: Amount of fuel energy and exergy in kJ exhausted, destroyed and converted to work and heat transfer for the current operating condition.

In terms of percentage energy and exergy distribution the percentage of expansion work is higher for energy compared to exergy. This is because of the difference in the fuel heating value and chemical exergy value. The trend is the same for heat transfer as in figure 27. The percentage of energy exhausted is higher than the percentage of exergy exhausted. A sizable fraction (almost 15%) of exergy is destroyed while all of the energy is conserved.

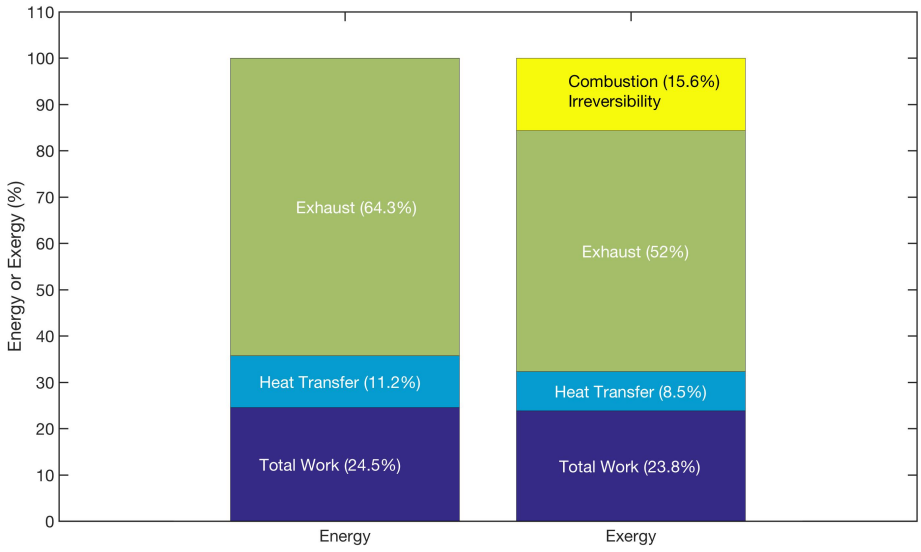

Figure 28: Percentage of fuel energy and exergy exhausted, destroyed and converted to work and heat transfer for the current operating condition.

From the bar chart in figure 28 we can compute the first law and second law efficiencies of the engine. The first law efficiency is a ratio of the useful work outputted to the chemical energy available in the fuel. It is computed as follows:

$$\eta_I = \frac{Total\ Indicated\ Work}{m_{fuel} Q_{LHV}} = \frac{3.68kJ}{0.0003kg\ 50.01MJ/kg} = 24.5\% \qquad (43)$$

The second law efficiency is a ratio of the useful work outputted to the chemical exergy available in the fuel. It is computed as follows:

$$\eta_{II} = \frac{Total\ Indicated\ Work}{m_{fuel} a_{fuel}} = \frac{3.68\ kJ}{0.0003kg\ 51.72MJ/kg} = 23.7\% \qquad (44)$$

The second law efficiency is less than the first law efficiency because the useless fraction of energy in the shape of irreversibility is accounted for in its calculation. It is thus, a better metric to quantify the performance of the engine at utilizing available energy.

5. SUMMARY AND CONCLUSION

The current study was started with the motivation of developing an in-house, computationally inexpensive and versatile modeling platform to study the thermodynamic performance of a legacy two stroke, large bore, natural gas fueled engine. These engines have been around since the mid twentieth century and because they were designed in the pre-emissions regulation days, their emissions performance is not up to par with the stringent regulations of today. Knowledge about the thermodynamic behavior of the engine would help in introducing design improvements that would improve the emissions performance of the engine.

With these objectives in mind a thermodynamic model was developed for the engine to simulate engine behavior at full load condition. Both the closed portion and open portion of the cycle were modeled using theories of gas dynamics, thermodynamics, heat transfer and associated fields. Salient features of the model have been summarized below:

- The closed system model simulates compression, combustion and expansion of these trapped cylinder gases. The accompanying heat loss to the wall is also accounted for using the Woschni correlation.
- Cylinder gases have been simulated using a two-zone modeling approach. There is an unburned zone and a burned zone, which develops once combustion starts.

As combustion continues the burned zone entrains more gases from the unburned zone until all that is left is burned combustion products.

- Combustion is modeled using a Weibe function to describe the mass fraction burn rates. Weibe parameters are tuned against experimental mass fraction burn curves.
- The model is a zero-dimensional model with no spatial resolution. There is uniformity in thermodynamic properties within each zone.
- The open system of the model simulates the gas exchange process between the engine cylinder, stuffing box and exhaust piping. Scavenging performance of the engine can be assessed from the simulated cylinder mass flows.
- Gas flows across inlet and exhaust ports are modeled using equations for non-isentropic flows with empirically known coefficients of discharge for the ports and experimentally determined pressure values for stuffing box and exhaust manifold.

The model discussion describes the basic framework model which serves as a platform for specialized sub-models to investigate specific engine performance parameters of interest e.g. emissions generation, combustion phasing etc. The key parameter investigated in this study was the exergy performance of the engine. Exergy quantifies the potential of doing useful work that energy being transferred carries. Knowledge about exergy utilization distribution in an engine and the contribution of

various modes of exergy transfer and destruction can provide useful insights about the sources of wastage of useful energy in the system.

Figures 27 and 28, which describe the distribution of energy and exergy utilization in the engine, are the most important results from this investigation. In figure 29 the results from this study and a similar study by Caton [23] on a 5.7litre, V-8 four-stroke engine have been shown. As hypothesized earlier in the literature review section the percentage of exergy destroyed is lower for the two stroke engine at the current operating point compared to its four stroke counterpart (15.6% vs. 20%). This is so because the mean effective pressures were higher in the two-stroke engine. For the energy and exergy distribution the percentage of expansion work is higher for energy compared to exergy. The percentages of energy and exergy transfer with heat transfer are lower in case of the two-stroke engine (11% vs. 23.7% and 8.5% vs. 19.2%). This is probably because of the lower gas temperatures in the two stroke engine cylinder. Because the fraction of exergy destroyed and exergy transferred with heat transfer is lower for the two-stroke engine the amount of exergy carried out along with the exhaust gases is higher than that in the case of the four-stroke engine (52% vs. 27.2%). The same is true for energy transfers as well (64.3% vs. 44.1%).

(i)

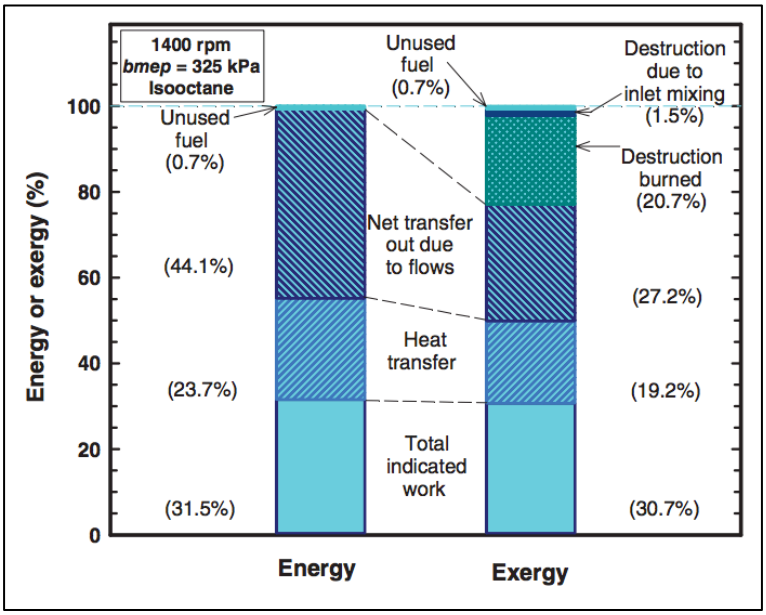

(ii)

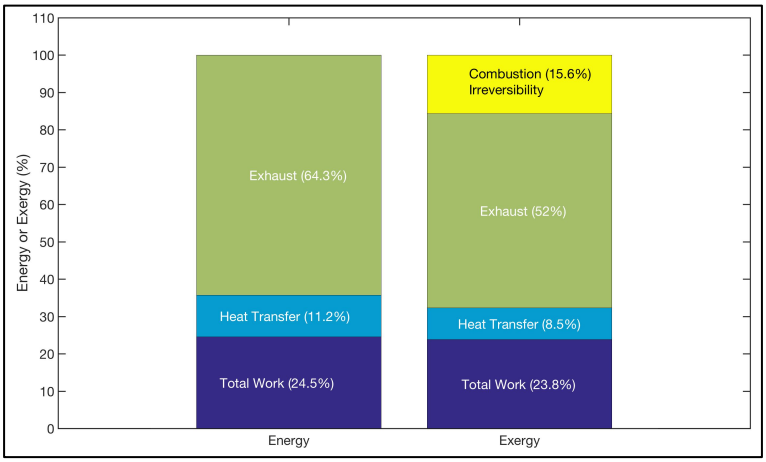

Figure 29: Percentage of fuel energy and exergy exhausted, destroyed and converted to work and heat transfer for (i) a four-stroke engine [23] and (ii) the two-stroke engine being studied.

Similar results have been presented by Andrzej and Zhang [5] for two different fuels fueling a 4.7 liter, V8 four-stroke engine, namely: gasoline and CNG These are shown in figure 30. Exergy destruction is again higher in the four-stroke case, but the

difference is lower for the case with CNG. Exergy transfer with heat transfer has the same trend. Exergy loss to the environment is lower for the four-stroke engine.

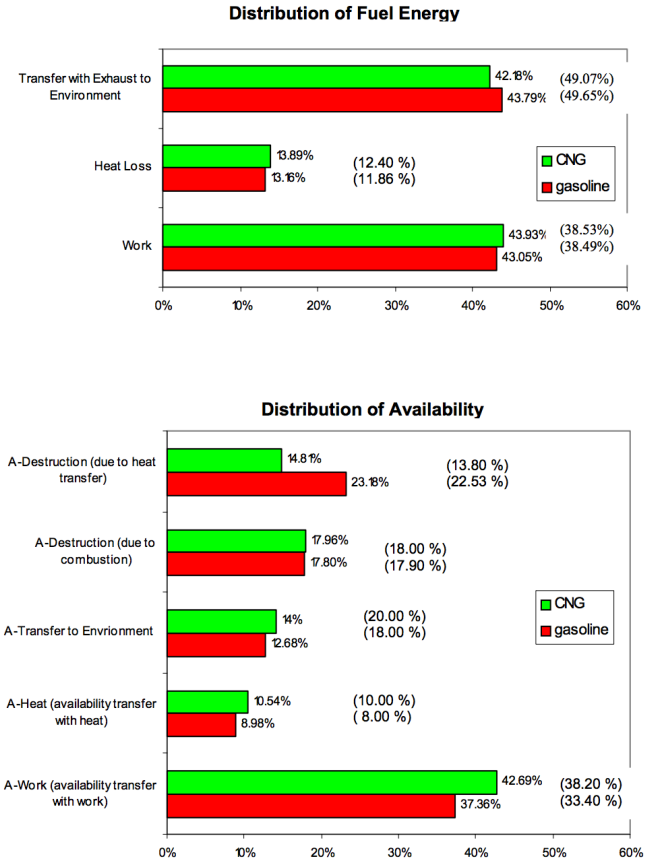

Figure 30: Fuel energy and exergy distribution for a four-stroke engine fueled by gasoline and CNG [5].

In conclusion, insights regarding exergy distribution operating at rated load and speed were gained through this study. Even though, comparison of these findings with findings from similar studies carried on four stroke engines brought to light some interesting distinctions between the exergy utilization modes in the two cases, a more insightful comparison would be one between different operating conditions of the same

engine. This is something that will be looked into in the future when experimental data is available for different operating points. Some other recommendations for future investigations are listed below:

- Expanding the second law analysis to the whole cycle, rather than just the closed portion.
- Studying emissions generation in the engine by coding in the required sub-models.
- Studying the gas exchange performance of the engine by developing more detailed gas exchange models and supplementing those with experimental gas exchange studies.
- Probing the impact of non-methane fuel fractions in the fuel on exergy utilization behavior of the engine.

REFERENCES

[1] Blair, Gordon P. Design And Simulation Of Two-Stroke Engines. Warrendale, PA: Society of Automotive Engineers, 1996.

[2] Kojima, Masami, Carter Brandon, and Jitendra J. Shah. Improving urban air quality in South Asia by reducing emissions from two-stroke engine vehicles. No. 21911. World Bank, 2000.

[3] AJAX Products Group. Description of AJAX Engines. Cameron Corporation, 1963.

[4] Heywood, John B., and Eran Sher. The Two-Stroke Cycle Engine. Warrendale, PA: Society of Automotive Engineers, 1999. 472 (1999).

[5] Sobiesiak, Andrzej, and Shengmei Zhang. The first and second law analysis of spark ignition engine fuelled with compressed natural gas. No. 2003-01-3091. SAE Technical Paper, 2003.

[6] Heywood, John B., et al. Development and use of a cycle simulation to predict SI engine efficiency and NOx emissions. No. 790291. SAE Technical Paper, 1979.

[7] Raine, R. R., C. R. Stone, and J. Gould. Modeling of nitric oxide formation in spark ignition engines with a multizone burned gas. Combustion and Flame 102.3: 241-255, 1995.

[8] Heywood, John B. Combustion and its modeling in spark-ignition engines. International Symposium COMODIA. Vol. 94. 1994.

[9] Morel, Thomas, et al. Model for heat transfer and combustion in spark ignited engines and its comparison with experiments. No. 880198. SAE Technical Paper, 1988.

[10] Krieger, R. B., and Gary L. Borman. Computation of apparent heat release for internal combustion engines. Mechanical Engineering. Vol. 89. No. 1. 345 E 47th st, New York, NY 10017: ASME-AMER SOC Mechanical Eng, 1967.

[11] Van Gerpen, J. H., and H. N. Shapiro. Second-law analysis of diesel engine combustion. Journal of Engineering for Gas Turbines and Power 112.1: 129-137, 1990.

[12] Flynn, P. F., et al. A new perspective on diesel engine evaluation based on second law analysis. No. 840032. SAE Technical Paper, 1984.

[13] Zheng, Junnian, and Jerald A. Caton. Use of a single-zone thermodynamic model with detailed chemistry to study a natural gas fueled homogeneous charge compression ignition engine. Energy Conversion and Management 53.1: 298-304, 2012.

[14] Rakopoulos, C. D., and D. C. Kyritsis. Comparative second-law analysis of internal combustion engine operation for methane, methanol, and dodecane fuels. Energy 26.7: 705-722, 2001.

[15] Ferguson, Colin R., and Allan T. Kirkpatrick. Internal Combustion Engines: Applied Thermosciences. John Wiley & Sons, 2015.

[16] Caton, Jerald A. A multiple-zone cycle simulation for spark-ignition engines: thermodynamic details. Large-Bore Engines, Fuel Effects, Homogeneous Charge Compression Ignition, Engine Performance And Simulation 2: 37-2, 2001.

[17] Caton, Jerald A. A cycle simulation including the second law of thermodynamics for a spark-ignition engine: implications of the use of multiple-zones for combustion. No. 2002-01-0007. SAE Technical Paper, 2002.

[18] Ramos, J. I. Comparisons between thermodynamic and one-dimensional combustion models of spark-ignition engines. Applied Mathematical Modelling 10.6: 409-422, 1986.

[19] Shapiro, Howard N., and Jon H. Van Gerpen. Two zone combustion models for second law analysis of internal combustion engines. No. 890823. SAE Technical Paper, 1989.

[20] Kong, Song-Charng, Zhiyu Han, and Rolf D. Reitz. The development and application of a diesel ignition and combustion model for multidimensional engine simulation. No. 950278. SAE Technical Paper, 1995.

[21] Verhelst, Sebastian, and C. G. W. Sheppard. Multi-zone thermodynamic modelling of spark-ignition engine combustion–an overview. Energy Conversion and Management 50.5: 1326-1335, 2009.

[22] Bayraktar, Hakan. Mathematical modeling of spark-ignition engine cycles. Energy Sources 25.5: 439-455, 2003.

[23] Caton, Jerald A. An Introduction to Thermodynamic Cycle Simulations for Internal Combustion Engines. John Wiley & Sons, 2015.

[24] Woschni, Gerhard. A universally applicable equation for the instantaneous heat

transfer coefficient in the internal combustion engine. No. 670931. SAE Technical paper, 1967.

[25] Heywood, John B. Internal Combustion Engine Fundamentals. Vol. 930. New York: Mcgraw-Hill, 1988.

[26] Blizard, Norman C., and James C. Keck. Experimental and theoretical investigation of turbulent burning model for internal combustion engines. No. 740191. SAE Technical Paper, 1974.

[27] Morel, Thomas, et al. Model for heat transfer and combustion in spark ignited engines and its comparison with experiments. No. 880198. SAE Technical Paper, 1988.

[28] Caton, Jerald A. Comparisons of global heat transfer correlations for conventional and high efficiency reciprocating engines. ASME 2011 Internal Combustion Engine Division Fall Technical Conference. American Society of Mechanical Engineers, 2011.

[29] Nusselt, W. Der Wärmeübergang in der Verbrennungs-kraftmaschine, V. D. I.-Forschungsheft, 264, 1923.

[30] Annand, W. J. D. Heat transfer in the cylinders of reciprocating internal combustion engines. Proceedings of the Institution of Mechanical Engineers177.1 1963: 973-996, 1963.

[31] Woschni, Gerhard. A universally applicable equation for the instantaneous heat transfer coefficient in the internal combustion engine. No. 670931. SAE Technical paper, 1967.

[32] Hohenberg, Günter F. Advanced approaches for heat transfer calculations. No. 790825. SAE Technical paper, 1979.

[33] Heywood, John B., and Eran Sher. The Two-Stroke Cycle Engine. Warrendale, PA: Society of Automotive Engineers, 1999. 472, 1999.

[34] Annand, Walter John Dinnie, and Geoffrey Ernest Roe. Gas Flow In The Internal Combustion Engine: Power, Performance, Emission Control, And Silencing. London: GT Foulis, 1974.

[35] Wallace, W. B. Paper 4: High-output medium-speed diesel engine air and exhaust system flow losses. Proceedings of the Institution of Mechanical Engineers, Conference Proceedings. Vol. 182. No. 4. SAGE Publications, 1967.

[36] Benson, R. S. Experiments on a piston controlled port. The Engineer 210 875-880, 1960.

[37] John, James EA. Gas Dynamics. Pearson Education India, 1969.

[38] Sher, Eran. Scavenging the two-stroke engine. Progress in Energy and Combustion Science 16.2 95-124, 1960.

[39] Benson, Rowland S., W. J. D. Annand, and P. C. Baruah. A simulation model including intake and exhaust systems for a single cylinder four-stroke cycle spark ignition engine. International Journal of Mechanical Sciences 17.2 97-124, 1975.

[40] Benson, Rowland S., and Peter T. Brandham. A method for obtaining a quantitative assessment of the influence of charging efficiency on two-stroke engine performance. International Journal of Mechanical Sciences 11.3: 303-312, 1969.

[41] Maekawa, M., Text of course, JSME G36, 23,1957.

[42] Benson, Rowland S. A new gas dynamic model for the gas exchange process in two stroke loop and cross scavenged engines. International Journal of Mechanical Sciences 19.12: 693-711, 1977.

[43] Kishan, S., S. R. Bell, and J. A. Caton. Numerical simulations of two-stroke cycle engines using coal fuels. Journal Of Engineering For Gas Turbines And Power 108.4 : 661-668, 1986.

[44] Griffin, Aaron A., Mashayekh Alireza and Timothy J. Jacobs. experimental and simulated pressure measurements of a two stroke large bore natural gas spark ignited engine. Gas Machinery Conference 2015. Gas Machinery Research Council, 2015.

[45] Moran, Michael J. Availability Analysis: A Guide To Efficient Energy Use. ASME Press, 1982.

[46] Moran, Michael J., Moran, M. J., Shapiro, H. N., Boettner, D. D., & Bailey, M. B. Fundamentals of Engineering Thermodynamics. John Wiley & Sons, 2010.

[47] Caton, Jerald A. A review of investigations using the second law of thermodynamics to study internal-combustion engines. No. 2000-01-1081. SAE Technical Paper, 2000.

[48] Rakopoulos, C. D., and E. G. Giakoumis. Second-law analyses applied to

internal combustion engines operation. Progress in Energy and Combustion Science 32.1: 2-47, 2006.

[49] Caton, Jerald A. Operating characteristics of a spark-ignition engine using the second law of thermodynamics: effects of speed and load. No. 2000-01-0952. SAE Technical Paper, 2000.

[50] Sezer, İsmet, and Atilla Bilgin. Mathematical analysis of spark ignition engine operation via the combination of the first and second laws of thermodynamics. Proceedings of the Royal Society of London A: Mathematical, Physical and Engineering Sciences. Vol. 464. No. 2100. The Royal Society, 2008.

[51] Bejan, M. J., and G. Tsatsaronis. Moran, Thermal Design and Optimization. John Wiley and Sons, 1996.

[52] Rodríguez, Luis. Calculation of available-energy quantities. ACS Symposium Series, Vol. 122 39-59, 1980.

[53] Stepanov, V. S. Chemical energies and exergies of fuels. Energy 20.3 1995: 235-242, 1995.

[54] Caton, Jerald A. On the destruction of availability (exergy) due to combustion processes—with specific application to internal-combustion engines. Energy 25.11: 1097-1117, 2000.

[55] Gordon, Sanford, and Bonnie J. McBride. Computer Program for Calculation of Complex Chemical Equilibrium Compositions, Rocket Performance, Incident and Reflected Shocks, and Chapman-Jouguet Detonations. Interim Revision, March 1976, 1976.

[56] Kee, Robert J., Fran M. Rupley, and James A. Miller. The Chemkin thermodynamic data base. Sandia National Laboratories Report SAND87-8215B, 1990.

[57] Stone, Richard. Introduction To Internal Combustion Engines. SAE International, 1999.

[58] Chase, Malcolm W. JANAF thermochemical tables. JANAF thermochemical tables, by Chase, MW Washington, DC: American Chemical Society; New York: American Institute of Physics for the National Bureau of Standards, c1986. United States. National Bureau of Standards. 1, 1986.

[59] Olikara, Cherian, and Gary L. Borman. A computer program for calculating

properties of equilibrium combustion products with some applications to IC engines. No. 750468. SAE Technical Paper, 1975.

[60] Griffin, Aaron A., and Timothy J. Jacobs. Combustion characteristics of a 2-stroke large bore natural gas spark-ignited engine. ASME 2015 Internal Combustion Engine Division Fall Technical Conference. American Society of Mechanical Engineers, 2015.

[61] Griffin, Aaron A. Combustion Characteristics of a Two-Stroke Large Bore Natural Gas Spark-Ignited Engine. Diss. Texas A&M University, 2015.

[62] Benson, R.S., Baruah, P.C. and Whelan, B., 1975. Simulation model for a crankcase-compression two-stroke spark-ignition engine including intake and exhaust systems. Proceedings of the Institution of Mechanical Engineers,189(1), pp.167-175, 1975.

[63] Simpson, Adam P., and Andrew E. Lutz. Exergy analysis of hydrogen production via steam methane reforming. International Journal of Hydrogen Energy 32.18 4811-4820, 2007.

[64] Kotas, Tadeusz Jozef. The Exergy Method Of Thermal Plant Analysis. Elsevier, 2013.